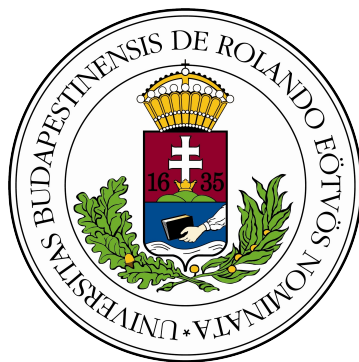


Thesis

Numerical investigation of
coincidence-correction in gamma
spectroscopy



by Bogye Balázs
Physics MSc, Eötvös Loránd University
Scientific data analysis and modelling specialization

Supervised by Dr. Horváth Ákos
Associate Professor, Eötvös Loránd University
Department of Atomic Physics

2021. May

NYILATKOZAT

Név: Bogye Balázs

ELTE Természettudományi Kar, szak: Fizikus MSc

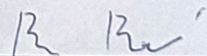
NEPTUN azonosító: B8KE4G

Diplomamunka címe:

Numerical investigation of coincidence-correction in gamma spectroscopy

A **diplomamunka** szerzőjeként fegyelmi felelősségem tudatában kijelentem, hogy a dolgozatom önálló szellemi alkotásom, abban a hivatkozások és idézések standard szabályait következetesen alkalmaztam, mások által írt részeket a megfelelő idézés nélkül nem használtam fel.

Budapest, 2021. 05. 31



a hallgató aláírása

Abstract

For precise activity analysis of radioactive isotopes the inclusion of gamma coincidence correction is necessary. The summing-in and summing-out effects caused by gamma cascades can distort the spectrum. Without coincidence correction these effects lead to systematic errors in the analysis.

Here I investigate the effect of coincidence correction on an HPGe detector using the Semkow matrix formalism. To do this I simulate the detector using Geant4 to calculate it's efficiency curves, build the correction matrices and calculate the corrected relative intensities. I also analyse an existing measurement's spectrum and apply the correction terms to the peaks of ^{208}Tl . The activity correction is found to be +25%.

Acknowledgements

I would like to say thanks to my supervisor, Horváth Ákos, for his help and guidance, for accepting me for this thesis and for his availability (even on weekends and at night) and intensive co-operation in the last three weeks.

I would like to thank my partner for her infinite patience and emotional support, and also for continuously nagging me to finally finish this. I am thankful for the support of my family, especially my mother, (yet again) for not letting me leave my studies unfinished.

I also express my gratitude to my boss and my employer for allowing me a 3-week unpaid leave to let me concentrate on writing so I could finish on time.

Contents

1	Introduction	2
2	Coincidence summing	4
2.1	Coincidence summing effect	4
2.2	Coincidence summing in literature	5
2.3	Semkow matrix formalism	5
2.3.1	Transition probabilities	6
2.3.2	Detection probabilities	7
2.3.3	Cascade probabilities	8
2.3.4	Peak area correction	9
2.3.5	$\mu \rightarrow 0$ limit	10
3	Geant simulation of HPGe detector	11
3.1	Geant	11
3.2	Detector	13
3.3	Program	14
3.3.1	Geometry used	15
3.3.2	Physics processes	17
3.3.3	Particle source	18
3.3.4	Measured quantities	18
3.4	Validations	19
4	Construction of the matrices	23
4.1	Simulation efficiency results	23
4.1.1	Simulation parameters	23
4.1.2	100 keV - MeV range	23
4.1.3	25 keV - 25 MeV range	24
4.1.4	Efficiency distance dependence	26
4.2	Construction of matrices for ^{208}Tl	30
4.2.1	Transition probability matrix	30
4.2.2	Corrected intensities	32
5	Applying to ^{208}Tl measurement	35
5.1	Measurement	35
5.2	Fitting peaks of experimental data	35
5.3	Activity correction	39
5.3.1	Activity at 2mm distance correction	39
5.3.2	Activity over distance	41
6	Summary	43
A	Appendix	47
A.1	Coincidence corrected intensities	47
A.2	Energy and distance dependent efficiencies	48

1 Introduction

Gamma spectroscopy is a widely used technique to determine the radioactive components and their activity in a sample. One of its applications is the analytical analysis of low activity environmental samples, such as detection and determination of the activity of uranium, thorium, etc. While knowing the relative intensity of the various gamma emissions and the efficiency of the detector at first sounds enough to calculate the activity of the source, there are other phenomena than emission and detection.

The photons after being emitted by the nucleus could end up getting absorbed in the sample (self-absorption), never leaving it and not getting detected, causing energy dependent detection efficiency decrease, Fig 1. The problem is further complicated by the fact that the exact composition of the material is not even known, so self-absorption cannot be exactly modeled.

Another problem is caused by gamma cascades. In gamma cascades photons are emitted from the nucleus a few nanoseconds apart, while the time resolution of the detector is about a few μs , possibly causing the emitted photons to be detected as a single one. Gamma coincidence, the detection of multiple gammas at once, is significant in high efficiency cases. As environmental samples have small activity, efficiency is kept as high as possible (e.g. via minimizing the sample distance) in order to shorten measurement time. The resulting coincidences deform the measured spectrum, leading to systematic errors and incorrect results.

In this work I investigate the effect of coincident summing in gamma cascades on the activity measurement of environmental samples, on the analytical determination of their ^{238}U , Th, etc. content. One solution for modelling the gamma cascades and applying their correction is the matrix model created by Semkow [2]. My goal is applying this model to the HPGe detector available at ELTE Department of Atomic Physics, the determination of the detector's efficiency on all energies with a Monte Carlo simulation, the calculation of the Semkow correction matrices for a given isotope (^{208}Tl) and carrying out the correction to a real measurement.

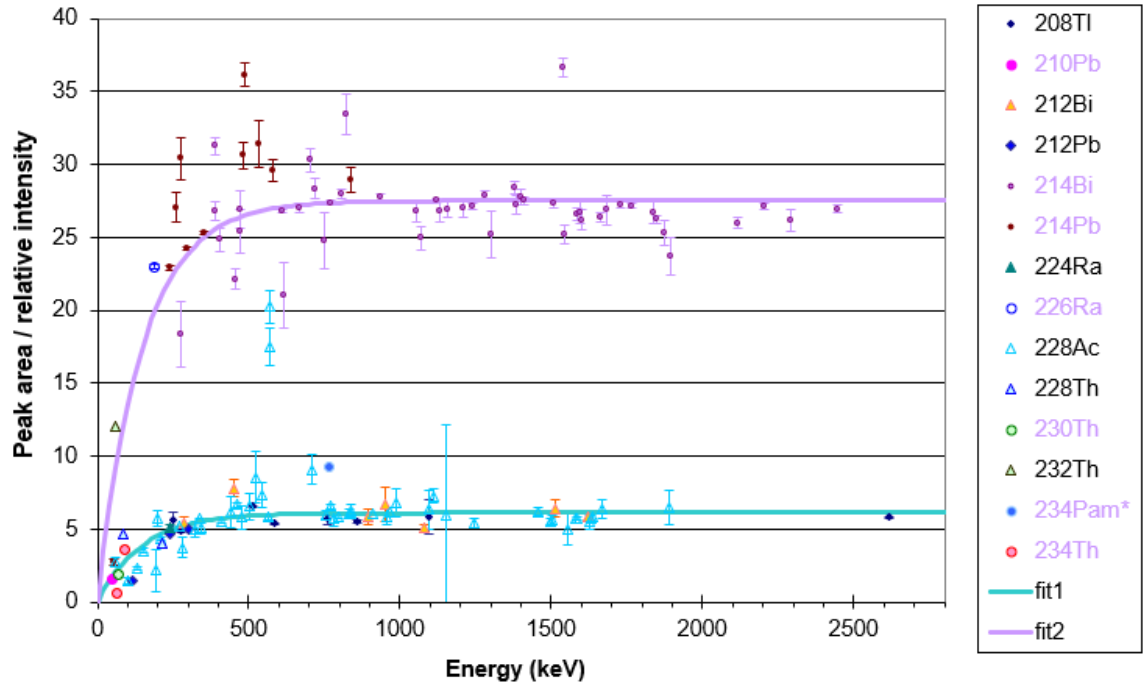


Figure 1: Peak area / literature relative intensity values over energy for an environmental sample measurement taken by a Compton suppression HPGe detector at KFKI and analyzed at ELTE Department of Atomic Physics (unpublished data).

Values calculated from all detectable peaks, separated into ^{232}Th and ^{238}U series isotopes. Both decay series fitted with an exponential curve. The calculated value ignoring gamma cascades would be a constant: activity times efficiency, but there is a serious fall in detection count at low energies accounted to self-absorption.

The origin of the outlier peaks is not clearly determined, it is suspected to be coincidence summing

2 Coincidence summing

2.1 Coincidence summing effect

Gamma detectors have a small but finite time resolution, a few μs are needed for the holes/electrons to reach the cathode/anode, the readout to collect the electrons generated in the crystal. Usually this doesn't cause problems as independent gammas are unlikely to coincidentally get detected within the same capture measurement window (without high enough activity) and even if they do the resulting energies will be smeared across the spectrum randomly. But this is not the case for gammas that are not independently getting coincided such as photons from cascades.

Gamma cascades (might) happen when a radioactive decay changes the nucleus (e.g. alpha or beta decay) leaving it in an excited state. While de-excitation of the nucleus could happen in a single gamma emission there are a number of other energy levels and it can happen along any allowed transition chain to the ground state. The half-time of these de-excitations is usually less than a few nanoseconds (often picoseconds), so even with 10-20 emissions it will almost certainly ($>99.9\%$) be over in less than a μs . This is not the case for meta-stable states, nuclear isomers, if their half life is comparable to the detector's time resolution (or larger) they can act just like stable states, and then cause a secondary cascade later. Apart from isomers the usual gamma cascade happens much faster than what the detector could differentiate so if multiple gammas get detected from a cascade only the sum of their deposited energy will be measured.

If a gamma gets fully absorbed but another gamma is detected with it then the first one will not be correctly counted (and neither will the second) resulting in a peak deficit, this is called summing-out.

On the other hand if two or more gammas get detected together then the sum of their energy could be the energy difference between two levels. This way they could be detected as a single transition, summing-in to that peak. This is of course especially the case with consecutive transitions in a cascade. Also it is worth noting that even energies of not allowed transitions can be measured due to summing-in.

So apart from the fast emissions, the phenomenon depends on multiple gamma detections (preferably all full energy absorption as otherwise the continuously distributed energy of partial absorption would smear the resulting energy distribution

into the Compton background). In order to have significant coincidences the detector's efficiency should be high enough, for one, the sample should be close enough. Or the other way around: to get rid of coincidences one could move the sample far away to lower the efficiency but it would also mean a lower hit-rate, in other words a longer measurement time.

All in all gamma coincidences can change the detected peak areas distorting our results, while it is possible to defend against it by moving the sample far away, this is not always a viable option, especially at low activity samples, so as a result we should incorporate this effect into our models and make the appropriate corrections when necessary.

2.2 Coincidence summing in literature

Coincidence summing has been handled by many authors. Andreev et al. [12, 13] created recursive formulas for handling coincidence for general β^- decays. McCallum et al. [14] modelled and analysed the distance dependence of coincidence correction, by factoring in the solid angle subtended by the detector corrected by energy and angle dependent attenuation. They also gave a solution for β^+ decay. Semkow et al. [2] derived the matrix notation form of Andreev's technique, which is easier to interpret and use, then calculated the corrected peak efficiencies by self-consistently iterating the correction terms for a measurement, he also showed that in complicated decay schemes the full correction term is needed, second order corrections are not enough. Sima [15] used a purely simulational Monte Carlo approach to calculate the ratio of coincidence corrected and uncorrected efficiency in environmental samples, taking into account the angular correlation of photons, showing that its effect can cause up to 10% difference at small detector solid angles, but it diminishes at low distances. His program was also able to take into account the efficiency distortion due to non-uniform source activity.

2.3 Semkow matrix formalism

I summarize here a version of the matrix formalism published by Semkow in 1990 [2], slightly modified by my advisor [16].

The transition among excitation levels in a gamma cascade is independent from the previous transitions, this way it can be modeled by a discrete Markov chain, where each step is a de-excitation.

Let n be the number of energy levels of the daughter nucleus (1 is ground, n is

highest possible level after decay), and let $\underline{p}^{(k)}$ be the probability vector of the state after k steps of gamma emission (p_i is the probability that the nucleus is in energy level i). Let the initial state be $\underline{p}^{(0)} = \underline{f}$, the feeding ratios / initial probability distribution of the nucleus.

2.3.1 Transition probabilities

Let X_{ij} be the probability that the next de-excitation from level j will go to level i , this way $(X^k)_{ij}$ gives us the chance that after k de-excitations from j the nucleus will be in state i . As transitions only happen to lower energy levels X is strictly upper triangular, so within $n - 1$ steps only stable states are populated.

Let M_{ij} be 1 if state $i = j$ is stable or is a metastable isomer (decay will be longer than detector time window) and 0 otherwise. This way $\underline{\underline{A}} = \underline{\underline{M}} + \underline{\underline{X}}$ gives our transition matrix, created this way so at stable and metastable states the transitions stop (of course $\sum_i X_{ij} = 1$, so $X_{ij} = 0$ if $X_{jj} = 1$ as there is no immediate next transition within the detector's time resolution). According to this the time (decay) evolution of the probabilities can be written as:

$$\underline{p}^{(k)} = \underline{\underline{A}}^k \underline{p}^{(0)}$$

Let V_{ij} be the matrix element describing the chance that the nucleus will go to level i after being on j along any possible path, not just directly. This can be expressed as getting there in 1, 2, ... $n - 1$ steps:

$$V_{ij} = \sum_{l=1}^n (X^l)_{ij}$$

$$\underline{\underline{V}} = \sum_{l=1}^{n-1} \underline{\underline{X}}^l$$

The transition from state j to i can happen different ways, not only with gamma decay, it could be internal conversion (emitting orbital electron instead of photon) or internal pair production (emitting electron-positron pair, instead of >1022 keV photon). As a result X is actually the sum of these three effects, that is

$$\underline{\underline{X}} = \underline{\underline{G}} + \underline{\underline{W}} + \underline{\underline{E}},$$

where G_{ij} is the probability of gamma, E_{ij} is of internal conversion, W_{ij} is of pair production transition from j to i in a single step. The various probabilities can be easily calculated knowing the decay rates, of course if there are other decays besides gamma (e.g. neutron emission) taking the nucleus from energy level j into a state

outside of the matrix (and stopping the investigated cascade) those effects should also be considered with a $\lambda^{(r)}$ rate. λ is the transition probability per unit time of different processes.

$$\begin{aligned}\lambda_{ij} &= \lambda_{ij}^{(g)} + \lambda_{ij}^{(w)} + \lambda_{ij}^{(e)} \\ \lambda_j &= \lambda^{(r)} + \sum_{i=1}^{j-1} \lambda_{ij} \\ x_{ij} &= \frac{\lambda_{ij}}{\lambda_j} \quad g_{ij} = \frac{\lambda_{ij}^{(g)}}{\lambda_j} \quad w_{ij} = \frac{\lambda_{ij}^{(w)}}{\lambda_j} \quad e_{ij} = \frac{\lambda_{ij}^{(e)}}{\lambda_j}\end{aligned}$$

The chance of getting to a given j state in any kind and number of steps (starting from \underline{f} distribution) equals q_j . The probability of a gamma transition from j to i energy level (ε_{ij}) therefore is calculated here, it is also called the relative intensity of that gamma photon (I_γ):

$$\begin{aligned}q_j &= f_j + \sum_{l=j+1}^n V_{jl} f_l \\ \varepsilon_{ij} &= q_j G_{ij}\end{aligned}$$

2.3.2 Detection probabilities

While we already have the probability of a single given energy transition we have not yet included the efficiency of the detector, as only a fraction of the photons going through it are detected. There are two types of efficiencies to differentiate, the full energy peak efficiency $\mu^{(P)}(E)$ (only gammas which got all of their energy absorbed) and the total efficiency $\mu^{(T)}(E)$ (gammas that had any interaction with the detector, in practice we use a cutoff energy under which everything is considered noise, so we have a lower energy limit too).

Both efficiencies are energy dependent, so each transition has its own efficiency. To handle this lets create $\underline{\underline{H}}^{(F)}$, $\underline{\underline{H}}^{(P)}$ and $\underline{\underline{H}}^{(N)}$ detection matrices, for the **full peak**, **partial energy deposited** and **no energy deposited** cases (the latter means in practice: less energy than the lower energy limit, mentioned above) .

$$\begin{aligned}
H_{ij}^{(F)} &= \mu^{(P)}(E_j - E_i) \\
H_{ij}^{(P)} &= \mu^{(T)}(E_j - E_i) - \mu^{(P)}(E_j - E_i) \\
H_{ij}^{(N)} &= 1 - H_{ij}^{(F)} - H_{ij}^{(P)}
\end{aligned}$$

Here E_i with 1 index is the energy of the i th state. Only $j > i$ transitions are valid, so these equations are only valid for $i < j$, otherwise the matrix elements are 0 (strictly upper triangle matrix).

Using these matrices the transition probabilities can be summed up as the sum of the three type of detection probabilities:

$$\underline{\underline{X}} = \underline{\underline{G}} + \underline{\underline{W}} + \underline{\underline{E}} = \underline{\underline{H}}^{(F)} \circ \underline{\underline{G}} + \underline{\underline{H}}^{(P)} \circ \underline{\underline{G}} + (\underline{\underline{H}}^{(N)} \circ \underline{\underline{G}} + \underline{\underline{W}} + \underline{\underline{E}}) = \underline{\underline{F}} + \underline{\underline{P}} + \underline{\underline{N}}$$

where \circ is the element-wise multiplication operation. The first part $\underline{\underline{F}} = \underline{\underline{H}}^{(F)} \circ \underline{\underline{G}}$ corresponds to the full peak detection probabilities of all transitions, $\underline{\underline{P}} = \underline{\underline{H}}^{(P)} \circ \underline{\underline{G}}$ is the same for partial detection (Compton plateau in the spectrum) and $\underline{\underline{N}}$ is the probability matrix for all transition to not get detected at all.

2.3.3 Cascade probabilities

Using the previously introduced transition detection probabilities one can easily find the cascade detection probabilities. The transition probability can be written as the sum of fully, partially and non-detected transitions:

$$\begin{aligned}
\underline{\underline{X}} &= \underline{\underline{F}} + \underline{\underline{P}} + \underline{\underline{N}} \\
\underline{\underline{X}}^k &= (\underline{\underline{F}} + \underline{\underline{P}} + \underline{\underline{N}})^k = \underline{\underline{F}}^k + \dots + \underline{\underline{N}}^k \\
\underline{\underline{V}} &= \sum_{l=1}^{n-1} \underline{\underline{X}}^l = \sum_{l=1}^{n-1} \underline{\underline{F}}^l + \sum_{l=1}^{n-1} \dots + \sum_{l=1}^{n-1} \underline{\underline{N}}^l = \tilde{\underline{\underline{F}}} + \tilde{\underline{\underline{P}}} + \tilde{\underline{\underline{N}}}
\end{aligned}$$

Where $\tilde{\underline{\underline{F}}} = \sum_{l=1}^{n-1} \underline{\underline{F}}^l$, $\tilde{\underline{\underline{P}}} = \sum_{l=1}^{n-1} \underline{\underline{P}}^l$ and $\tilde{\underline{\underline{N}}} = \sum_{l=1}^{n-1} \underline{\underline{N}}^l$ are the fully, partially and not detected partial cascade probability matrices (e.g. the probability of a cascade from state j to state i being fully detected, meaning all the transitions are detected as full energy peaks and $E_j - E_i$ energy is absorbed, is \tilde{F}_{ij}).

Any part of the sum containing a partial detection term $\underline{\underline{P}}$ with $\mu^{(P)}$ inside is summed into the partial sum (to keep it simple only written as "..." mid-calculation). The energy distribution of partial gamma detections is continuous, these partial detection products won't add much probability to the peaks, they will form the Compton

background. Although the terms with only $\underline{\underline{F}}$ and $\underline{\underline{N}}$ mixed inside $\tilde{\underline{\underline{P}}}$ are still giving sharp peaks.

2.3.4 Peak area correction

Now one can finally take into account the summing-in and out effects to find the area of the real peaks but with some assumptions.

As stated previously we will ignore the effect of partial detection for summing-in (for summing-out their effect is inherently included in the model).

We wish to find the $E_j - E_i$ "real peak"s' areas but of course we will find not only the $j \rightarrow i$ transition but all intermediate possible transitions summing-in (even if the $j \rightarrow i$ transition itself happens to be forbidden).

There will also be cascades in which some gammas won't be detected in the middle of the cascade and non-continuous transitions will leave energy, creating $(E_k - E_l) + (E_p - E_q) + \dots$ peaks, while it is theoretically possible that a combination of these could result in a $E_j - E_i$ real peak it is really unlikely and we will ignore it, assuming these transitions will always result in new peaks for which no single transition energy difference exists. Of course in real life application the validation of this claim is advised for the specific isotope.

To estimate the probability of all $E_j - E_i$ cascades with the previously mentioned assumptions we just have to calculate the probability of the system going to state j without any detection, then all transitions to i are all fully detected peaks (possibly summing-in) and after state i none of the transitions are detected again to level 1¹. Using the previously introduced $\tilde{\underline{\underline{F}}}$ and $\tilde{\underline{\underline{N}}}$ matrices the detection probability of $E_j - E_i$ peaks can be written as the product of the previously mentioned 3 phases, $O_{1,2,3}$:

$$\begin{aligned} O_1 &= f_j + \sum_{l=j+1}^n \tilde{N}_{jl} f_l \\ O_2 &= \tilde{F}_{ij} \\ O_3 &= \tilde{N}_{1i} \end{aligned}$$

Resulting in the hit count (B) for the $E_j - E_i$ energy peak:

$$B(E_j - E_i) = aO_1O_2O_3t$$

¹We assumed that state 1, the ground state, is the only stable or metastable state. If this is not the case we can't just write 1 and be done. We still have to sum for all possible [meta]stable ending states that are larger than i

where a is the activity of the source and t is the measurement time. Or in matrix form, with replacing the various indexed values with vectors and matrices:

$$\underline{\underline{B}} = a((\underline{O}_3 \otimes \underline{O}_1) \circ \underline{\underline{O}}_2)t,$$

where \otimes is the dyadic product (as \underline{O}_1 and \underline{O}_3 are vectors not matrices) and $B_{ij} = B(E_j - E_i)$.

2.3.5 $\mu \rightarrow 0$ limit

It can be shown that in the $\mu \rightarrow 0$ while μt stays constant limit (e.g. placing the detector further and measuring for a longer time) the simple formula:

$$B_{\text{simple}}(E_j - E_i) = a\varepsilon_{ij}\mu^{(P)}(E_j - E_i)t$$

As only the first order μ terms give a non-zero result, anything second or higher order can be ignored. So from $O_2 = \tilde{F}_{ij}$ only the first order term remains

$$O_2 = \tilde{F}_{ij} \approx F_{ij} = G_{ij}\mu^{(P)}(E_j - E_i),$$

which also means that from O_1 and O_3 not even first order μ terms can remain.

As $\mu \approx 0$ the detection terms are 0, so

$$N \approx X$$

$$\tilde{N} \approx V$$

$$O_1 \approx q_j$$

Also as V_{1i} is 1 as every state ends up on the ground state, so $O_3 = 1$. Resulting in

$$B(E_j - E_i) \approx aq_jG_{ij}\mu^{(P)}(E_j - E_i)t = a\varepsilon_{ij}\mu^{(P)}(E_j - E_i)t = B_{\text{simple}}(E_j - E_i)$$

This show that at small efficiencies the coincidence summing effects are insignificant.

3 Geant simulation of HPGe detector

3.1 Geant

Geant4 [3] is an open source toolkit for the simulation of the passage of particles through matter. For each run it starts with one or more primary particles then processes their movement and interactions by applying the user-chosen physics rules to the particles in each step (and substep).

Part of the simulation is the physics rules. Physics processes are applied to their specified particle types. The user can choose and define their own physics processes to use, there is no "one true physics", this is rather advantageous as one can try out different models, use simpler approximations / ignore unimportant phenomena to speed up their computations and remove complexity, or even write their own custom physics processes for special needs.

Physics processes are usually grouped into Physics Lists (e.g. EM, electromagnetic) which are then used in modules. For a quick start one can just choose a module/list fitting their general needs and ignore the details.

The user has to detail the geometry of their detector. This is done by defining its volume hierarchy. For each part 3 volumes are needed. The solid volume is just the geometrical shape and size of the object, the logical volume defines its material, visualization properties, etc. and all of these are put inside the physical volume. The physical volume puts the object into the object hierarchy, telling what other physical volume the object is inside of (e.g. detector is inside world, crystal volume is inside detector volume and so on) and their relative placement, repetition, etc. Daughter volumes must not protrude the mother volume.

The simulation is made up of runs. A run is a collection of events produced under identical conditions (geometry, physics).

Each run is made up of events, where the particle sources generate the primary particles and then the particles are advanced (according to physics) in steps until no tracks (current momentary particle states) are left in the stack (stack of tracks, the "list of all current particles"). Tracks are killed if they decay, get outside of the simulation world, come to a halt with no "AtRest" process acting on them or are killed by some user action/process.

Each step consists of 3 phases, pre-step, step (move, lose energy, etc.), post-step

(generate secondaries, remove track, etc.), physics processes can modify the particle, generate new ones, or even decide to kill it at each phase. Steps are always inside one volume (boundary crossing is a process too), the length of the step is determined by the processes acting on it, the process with the shortest interaction length limits the step length.

The user can create custom actions to inspect (and probably log/output) or modify the state of the simulation at various events. These actions are PrimaryGenerationAction, RunAction, EventAction, StackingAction, TrackingAction, SteppingAction.

The framework is able to control a vast amount of settings via macros, files giving an extra customization layer without requiring code compilation. Most programs can be started with a macro file as an input to execute it immediately (or without one to start GUI mode, where the user still can enter macro commands manually and start runs, etc.) The user can for example control the particle gun (energy, angle distribution, position), set the number of threads to run the simulation on in parallel, or execute any user defined command, etc.

3.2 Detector

The simulated detector is a GC1520-7500SL model **High Purity Germanium** detector, in use at ELTE. It has the measured outer dimensions of 7cm in length and 7.6cm in diameter, its crystal's dimensions from the specification are 42mm in length and 51mm in diameter, the crystal's distance from the end window is 5mm. It's inner composition, dimensions and exact placements are unknown but I could find a technical drawing, Fig 2, detailing the same detector model (although that one had slightly different crystal dimensions).

The detector has a resolution of 2 keV (FWHM) at 1.33 MeV and 1 keV at 122 keV based on the specifications, although in the measurement it seemed to be about 10-20% worse.

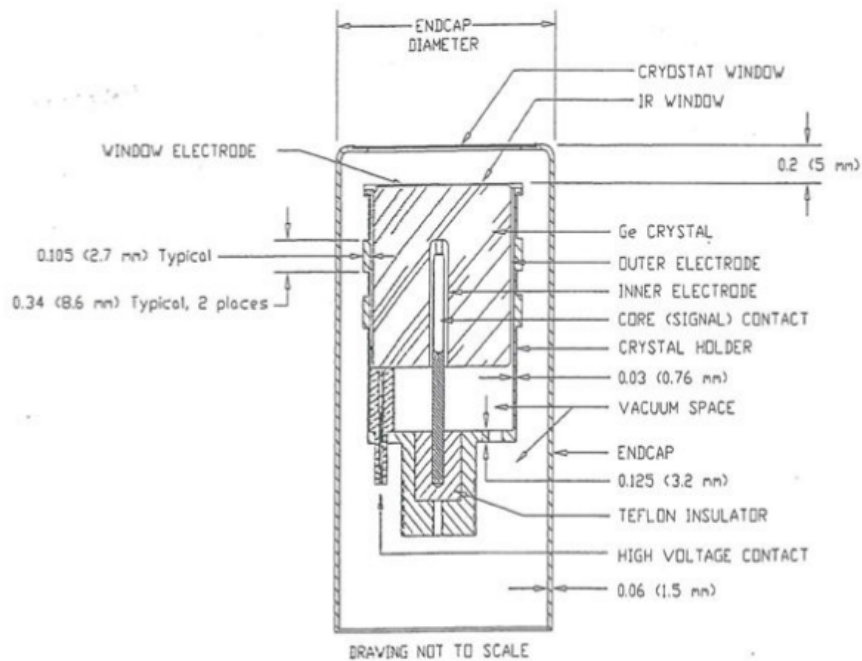


Figure 2: Technical drawing of GC1520 detector[4]

Drawing not to scale

3.3 Program

Geant itself is a library, not a program. To create the simulation I had to create a C++ program² that uses the Geant library, implementing the "standard" requirements a simulation needs, building the detector geometry, specifying physics, the particle source, creating my run/event/stepping actions, logging the required data, etc.

The various simulation scenarios all have their own Geant macros, and there are also a few helper python scripts to starting the simulations, reading the current setting's JSON config files, properly versioning the data and storing the setting's JSON with it too (mostly useful while the program was actively developed, the exact state of the simulation, both the code and the settings are saved automatically)³.

The program, macros for various runs, analysis notebook and most data can be found at <https://github.com/Balazzs/HPGECalorimeter>

I have done some additional simulations related to the HPGe gamma detection topic but not needed for the efficiency calculation, I will shortly mention some extra modes of the program, and some results in Section 3.4.

²The simulation was built on the skeleton of an existing Geant example project (B4a), but almost everything was changed

³A set of parametric runs (e.g. with varying sample distance) could also be started from an IPython notebook for ease of use. Unfortunately I lost the notebook itself, but the JSON interface it used is still working.

3.3.1 Geometry used

I have tried multiple geometries, first a simple 10cm, pure Ge cube for testing and then 3 different variations of the detector model. The exact dimensions and positions used in the simulation are described in `DetectorGeometry.cc` in the source.

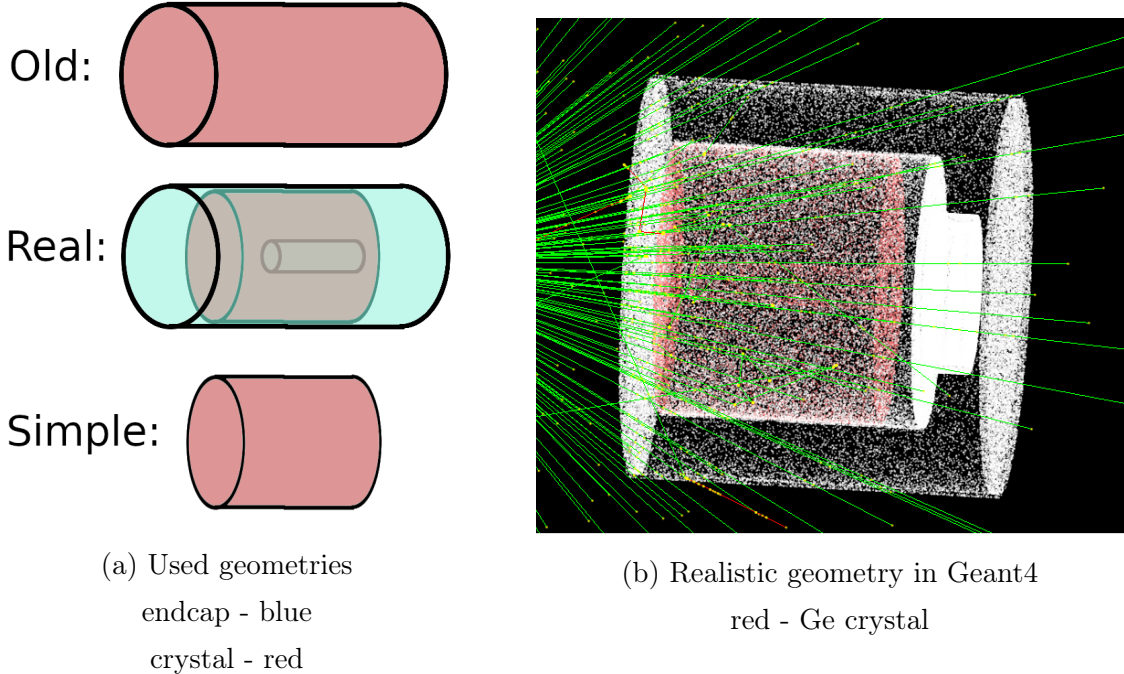
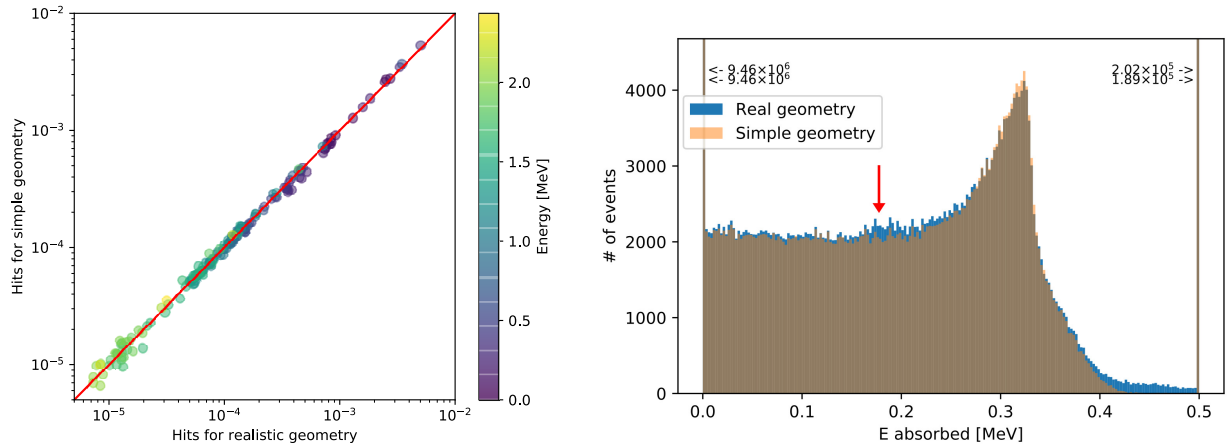


Figure 3: Detector geometry in simulation

The "old" model is simply assuming the detector is a Ge cylinder with its outer dimensions.

The "real" model is using the crystal dimensions from the technical specification, the outer size measurements for the end cap and some additional assumptions based on the technical drawing on Fig 2. In addition to the old method apart from correcting the crystal size it models the aluminium end cap, the inner crystal hole, and the Teflon insulator at the back end of the crystal.

I have also created a "simple" geometry where I only modeled the crystal core and ignored the end cap (and everything else) to investigate its effect on the simulation.



(a) Number of hits on various channels
 10^7 events, gamma from table
 No significant visible change

(b) Monoenergetic spectrum, 500 keV, 10^7 events
 Red arrow is expected backscatter position, the
 additional matter (aluminum end cap, Teflon
 insulation, etc.) makes backscattering possible,
 slightly changing the spectrum

Figure 4: Comparison of "simple" and "realistic" geometry for gamma sources

As seen in Fig 4b while the non-detecting matter of the detector is small compared to the crystal itself its effects are still visible on the spectrum. The backscatter peak is small but present, also the energy distribution seems to continuously reach the peak energy at 500keV while previously it stopped around 400keV.

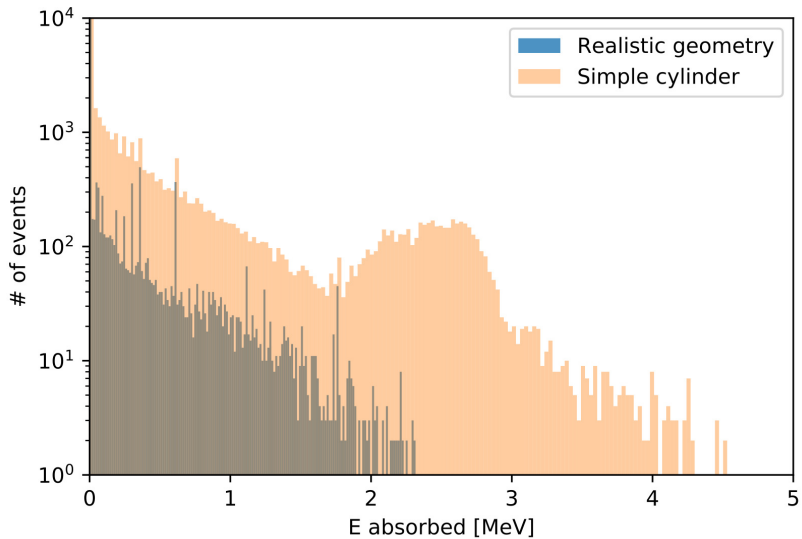


Figure 5: Spectrum of simulated decay in different geometries, 5 cm source distance. The end cap absorbs most charged particles generated in the simulated decay

Also in case of not just gammas being present, like the simulation of ^{238}U decay with RadioActiveDecayProcess the additional charged particles, electrons, alphas, etc. generate a tremendous number of hits if they enter, so the simulation of the end cap is a must have in this case, as seen on Fig 5.

The simulation also has a mode with a CaCO_3 sample holder (particle source and geometry need to be set independently) for simulating self-absorption.

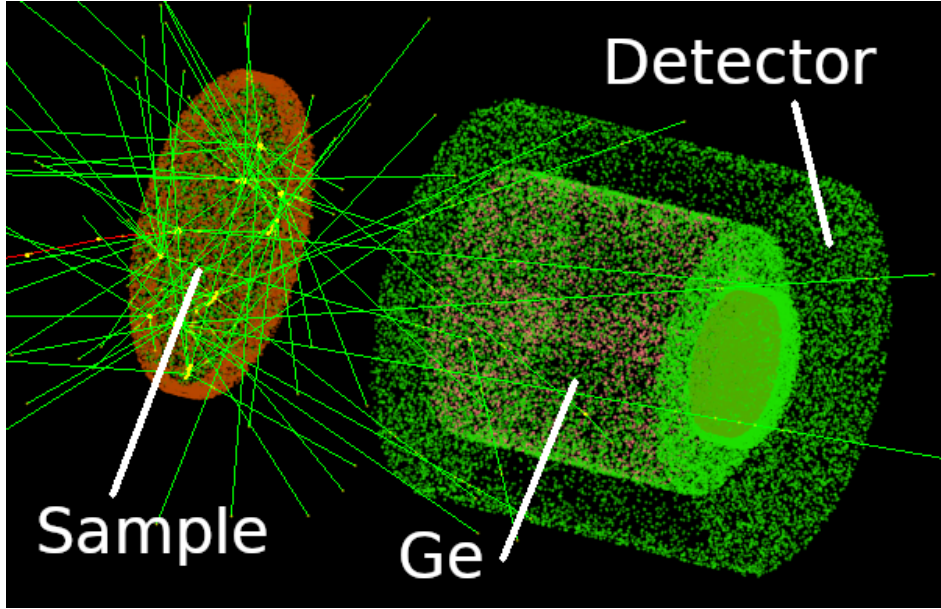


Figure 6: Sample (uniformly distributed source in CaCO_3 cylinder) in sample holder and detector with 10 simulated events

3.3.2 Physics processes

I am only interested in the electromagnetic phenomena happening, so I only added an electromagnetic physics list initially. The standard EM physics list is good for high energies but it is inaccurate at low energies[5]. There are low energy physics lists, like Livermore (data-driven) or Penelope (analytical, parametrized + data-driven), so I tried these and checked whether the change of physics truly has a significant effect on my simulation. At low energies ($\approx 100\text{keV}$, Fig 7) the standard EM list gives quite different results, but the 2 low energy lists mostly agree with each other, so I decided to use Penelope.

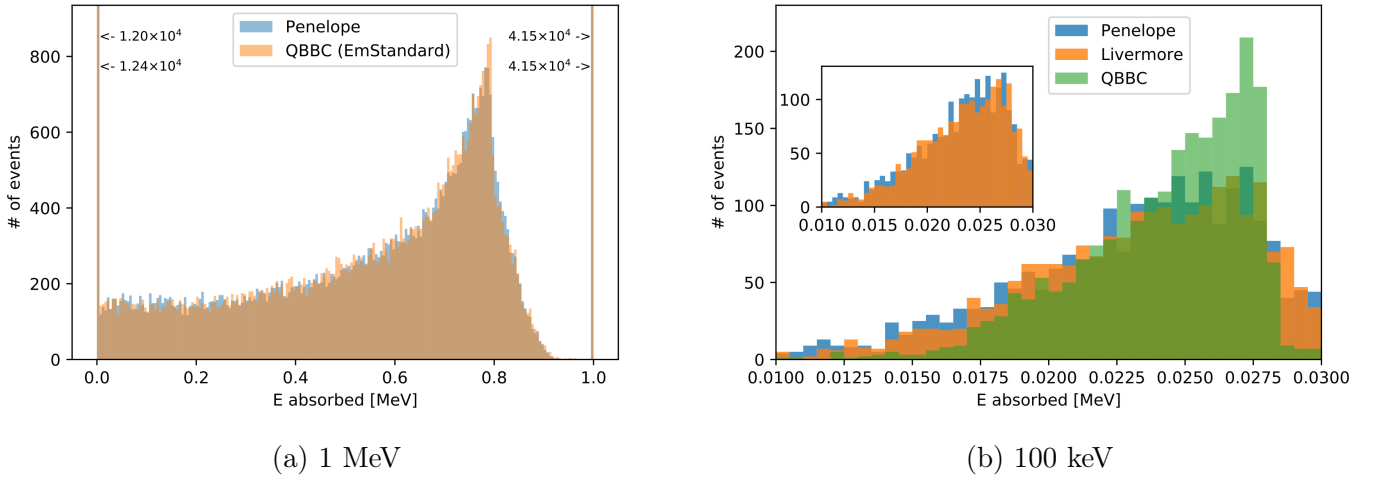


Figure 7: Gamma spectrum with different EM physics lists at various energies
 Old geometry, monoenergetic gamma, particle gun
 Texts show # of events at peaks outside of image

3.3.3 Particle source

I used the simulation to generate monoenergetic gammas or to simulate U238 decay. For the particle source I used **General Particle Source**, a highly adjustable particle source. The radial distribution of the source was set to be uniform on the half-sphere towards the detector (particles moving away from the detector are ignored, but compensated with a $\times 2$ multiplier). The energy distribution in case of gamma primaries was either constant for monoenergetic gammas or generated according to the probability distribution of ^{238}U gamma emissions, taken from literature[18], for ^{238}U gamma emission simulation.

There is also a third type of primary particle generation mode, when a ^{238}U isotope is created at rest and **RadioActiveDecayProcess** is added to the physics processes, letting Geant decay the ^{238}U isotope and leave the generation of gammas to it, this generates all daughter elements as a bonus, although it is computationally much more demanding.

3.3.4 Measured quantities

The program measures the energy deposited into the Ge crystal in each step via a custom **SteppingAction**, it sums the energy deposited and track length of charged particles in the crystal volume for every event. It also logs the exit momentum of the last photon leaving the simulation for each event and the energy of all newly created photons (through a custom **StackingAction**) throughout the entire run.

The measured energy, track length and exit angle are all collected into Geant NTuples and written to CSV files (one for each parallel thread). The photon creation energies are saved into a text file.

3.4 Validations

While creating the simulation and building it for the efficiency calculation I have checked a few other values and phenomena too. Some of them were used for validation of the simulation, others just seemed to be interesting. Here are a few of them that I used as an extra check to see if everything works fine.

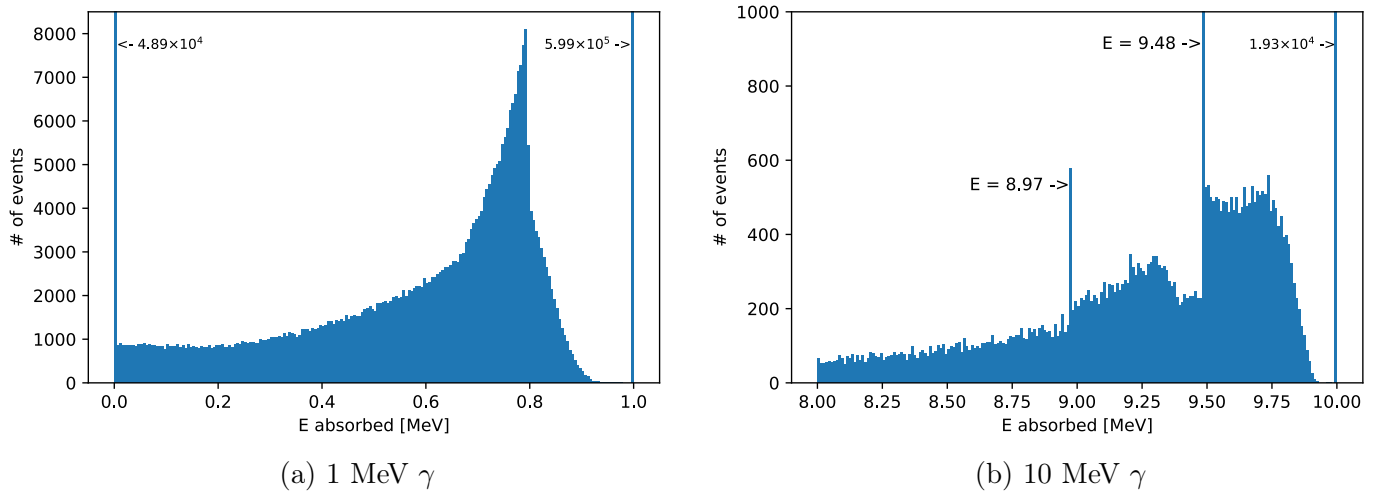


Figure 8: Gamma spectrum with $a=10\text{cm}$ cube detector

Texts show # of events at peaks outside of image

First I have checked a few simple monoenergetic gamma spectra (starting with the very first test geometry). The results seem to be correct, the photopeak (although being infinitely narrow as the readout is not simulated) and the Compton plateau are easy to see, on the >1022 keV spectra the single and double escape peaks (due to the electron, positron or both escaping from the detector after a pair production) are clearly discernible too.

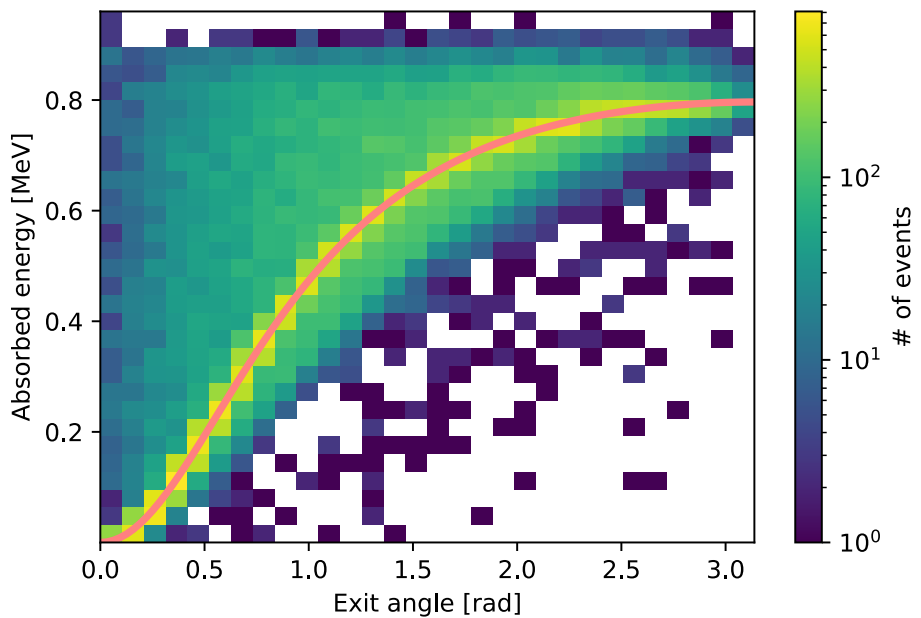


Figure 9: Exit angle vs energy absorption. 1 MeV photons
 Red curve is the theoretical energy deposit after a single Compton scattering⁴
 (Note the logarithmic scale)

At first I didn't understand the peak on Fig 8a at 0.8 MeV so I further investigated. There were not many physical processes happening in the detector. It was not photo-effect, the energy was too low for pair production, so I investigated the Compton scattering.

I checked the exit angle distribution of the (last) gamma ray exiting the detector, Fig 9, 10. Based on Fig 9 it becomes clear that the (small) peak is simply due to Compton scattering. The distribution closely resembles a single Compton scattering, and the absorbed energy over angle curve becomes flat at the $\approx 2 - \pi$ angle range, at $\approx 0.78\text{keV}$, so summing along this wide angle range a large portion of gamma is detected at around 0.8 keV, resulting in the peak.

⁴From the photon energy difference before and after scattering,
 $E_{\text{diff}} = E_\gamma \left(1 - \frac{1}{1 + (E_\gamma/m_e c^2)(1 - \cos \theta)}\right)$ where E_γ is the photon energy before scattering, θ is the angle and m_e is the electron's rest mass

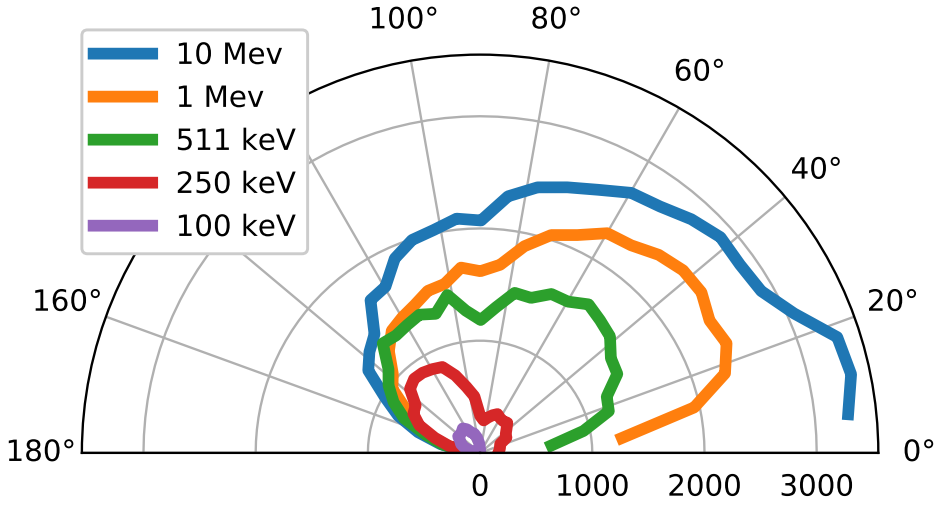


Figure 10: Exit angle distribution

0° not shown as great percent of photons didn't interact with the detector just flew through it at 0°

The distribution somewhat resembles the

Klein-Nishina cross sections[6]

For the source I had the ^{238}U gamma table generation that was validated by measuring the photon creation energies and comparing it to the table it was generated from, Fig 11. I also checked the gamma generation of the ^{238}U RadioActiveDecayProcess mode, Fig 12. The Geant decay process shows a good agreement with the table I got from literature, the only difference being the number of hits per event. The table generation mode creates a single photon from the energy distribution. Gammas are generated with their relative probability, this way coincidences are not present in table generation mode. On the other hand RadioActiveDecayProcess can generate multiple gamma per event, the ratio of photons created per event between the two modes was measured to be 2.177. This is in agreement with the sum of absolute probabilities in the generation table, which is 2.16, it lists only energies with a probability of 0.1% or more this is why the measured ratio is slightly more.

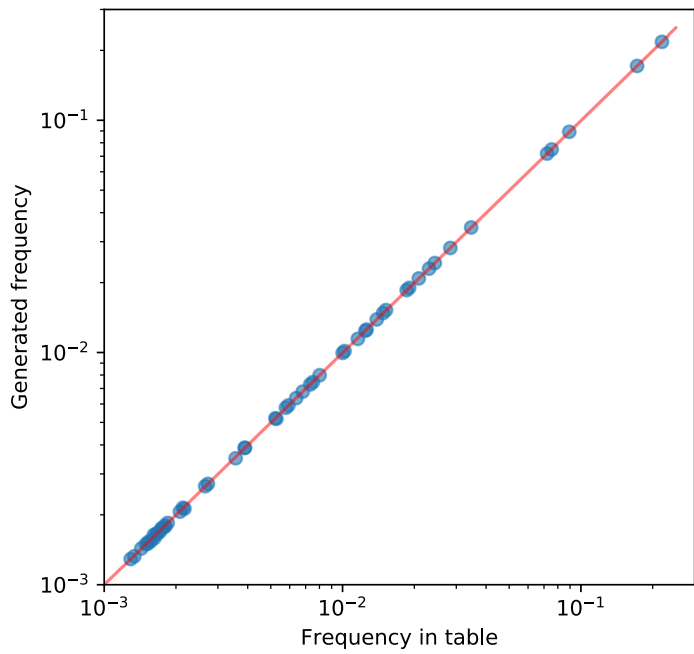


Figure 11: Validation of primary energy generation (and energy logging) with table source method
(frequency of various peak energies; 10m events)

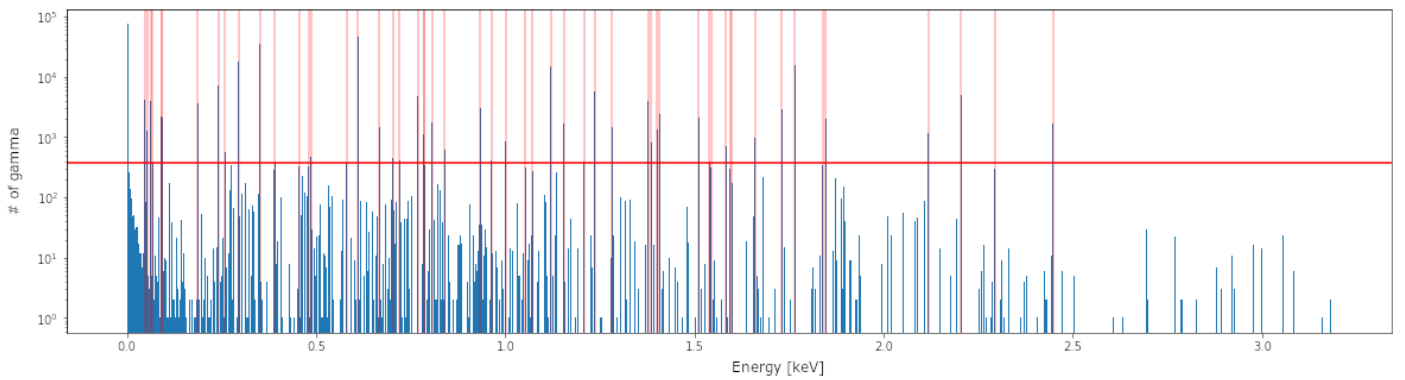


Figure 12: Simulated decay "primary" photon energies vs table photons
Blue bars are the number of simulated photons at various channels
Red vertical lines are photons in table
Red horizontal line is min frequency in table

4 Construction of the matrices

4.1 Simulation efficiency results

For the construction of the correction matrices the efficiency of each transition is required. The detector's efficiency depends on the gamma energy and of course on the detector's geometry. In order to determine its efficiency curve either many calibration measurements are needed with known energy peak isotopes over the whole range of energy or one could simulate the detector and the absorption of monoenergetic gammas, as I did.

4.1.1 Simulation parameters

The geometry and physics of the simulation were as described in Section 3.3 (Real geometry, Penelope physics list) the particle source used was the constant energy gamma point source. The detector sample distance was set to 5 cm as default. No sample container or additional sample geometry was used.

The logged absorbed energy per event values were not binned into channels to not distort the results. The photopeak efficiency was calculated from hits around the peak within a 5 keV radius (even though as there is no readout simulation the peaks are exact, not spread out). The total efficiency was calculated with 5 keV cutoff. While in experimental data it is advised to cut the low energy noise, in the simulation we do not have any noise. The low energy gammas can still coincide with other gamma absorptions so they do contribute to $\mu^{(T)}$ as long as they can move the detected energy out of its corresponding peak's range. I chose 5 keV as a small but larger than 0 cutoff.

4.1.2 100 keV - MeV range

Initially I simulated with primary energies from 100 keVs to MeV scale as most transitions are in this range⁵.

⁵In hindsight 3 MeV would have been better as the 2614 peak is one of the most important ones for Tl but I haven't decided on Tl at the time and the other fit was used in the end

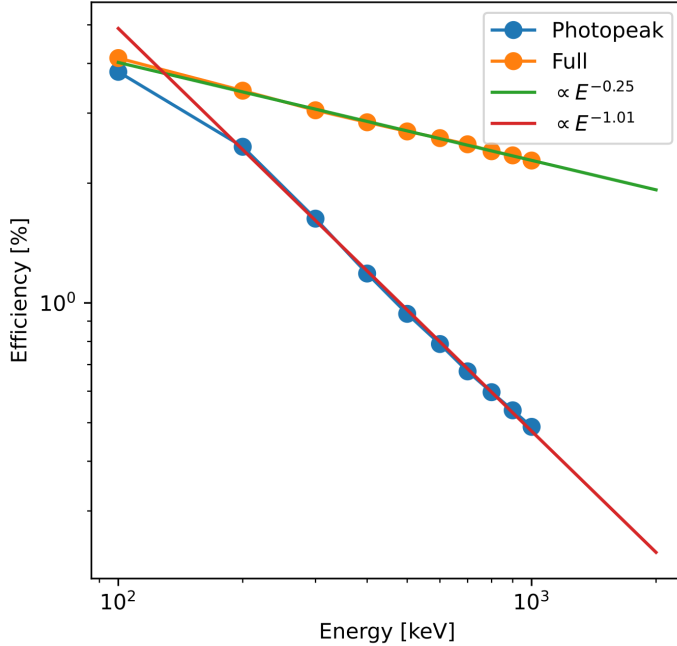


Figure 13: Simulated total and photopeak efficiency at various energies (narrow range) at 5 cm sample distance with power law fit. (log-log scale)

The efficiency curve is clearly energy dependent, and higher energies have lower efficiencies just as expected, as the cross section of Ge-gamma interaction is higher at lower energies (as the cross section of photoeffect falls with energy).

The curve seems to be a power law with a -0.25 scaling exponent for total efficiency and about -1 exponent for full peak efficiency, this seems to agree with literature[7]. While this is true from about 150 keV until about 3MeV, it is visible on Fig 13 that at ≈ 100 keV there is a deviation from this power law, to investigate this we need a wider energy range.

4.1.3 25 keV - 25 MeV range

I simulated at 12 energies over a wide range, starting from 25 keV until 25 MeV (25, 40, 60, 100, 150, 250, 400, 600, 1000, 1500, 2500, 4000, 6000, 10 000, 15 000, 25 000). While 10-20 MeV is already way out of our energy range it is required to see how the curve behaves at large energies. All runs consisted of 1 000 000 events. At every energy I ran 3 full runs⁶ with different random seed initialization, so the final efficiencies were calculated from 3 000 000 events.

⁶For 2 reasons: first and foremost because the simulation time of runs is rather long so running in smaller chunks is more manageable along my daily computer usage. Also this way I could double check that from all 3 sets of runs the efficiency results were the same

As seen on Fig 14 the power law behaviour only applies to the middle part of the range. On the left side of the curve at low energies the previously seen deviation starts around 150keV, and somewhere around 50 keV the curve turns around and lower energies are less likely to get detected. On the right side at about 4 MeV photo peak efficiency starts decreasing more rapidly.

Of course the total efficiency is always larger than the full peak efficiency, at low energies they are almost the same, showing that photoeffect is by far the most prominent effect in energy deposition. As photon energy grows Compton scattering becomes significant creating a division between the two efficiencies as gammas can exit the detector through scatterings. At 10-20 MeV total efficiency still doesn't seem to fall like photopeak, it even looks like there might be a small rising trend (although behaviour past these energies truly doesn't matter for this topic so the cause of this phenomenon was not investigated in detail).

In order to be able to get the efficiencies at any energy I had to fit the efficiency curve. A fifth order polynomial gives a good fit for it on log-log scale [7, 8].

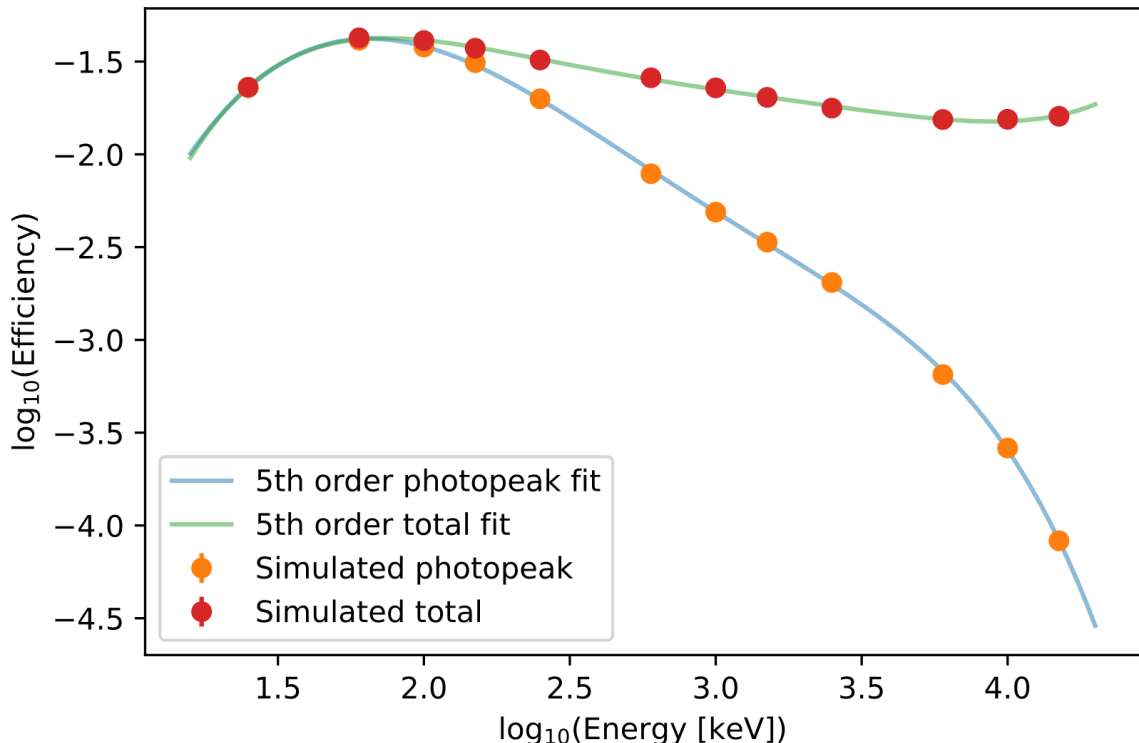


Figure 14: Simulated total and photopeak efficiency at various energies (wide range) with 5th order polynomial fit in log-log scale at 5 cm sample distance

4.1.4 Efficiency distance dependence

The detector-sample distance highly impacts the efficiencies, the farther the sample is the smaller the solid angle subtended by the detector becomes. For this reason the coincident correction method should take into account the sample distance, so I decided to fit the distance dependence of the efficiency curves too. (Or alternatively one could always simulate/measure the efficiencies at the exact distance where the sample is but then for every new experiment a new efficiency simulation/measurement is needed.)

I ran the same efficiency simulations as previously but now I reran it for a set of distances. I had 2 sets of runs, the first "large" distance one at 1, 3, 5, 10, 15, 20, 30, 40, 50, 60, 80, 100 mm distances and the second small distance one at 1, 1.25, 1.5, 1.75, 2, 2.25, 2.5, 2.75, 3, 3.5, 4, 4.5, 5, 6, 7, 8, 9, 10 mm distances. The simulated efficiencies are listed in Appendix A.2.

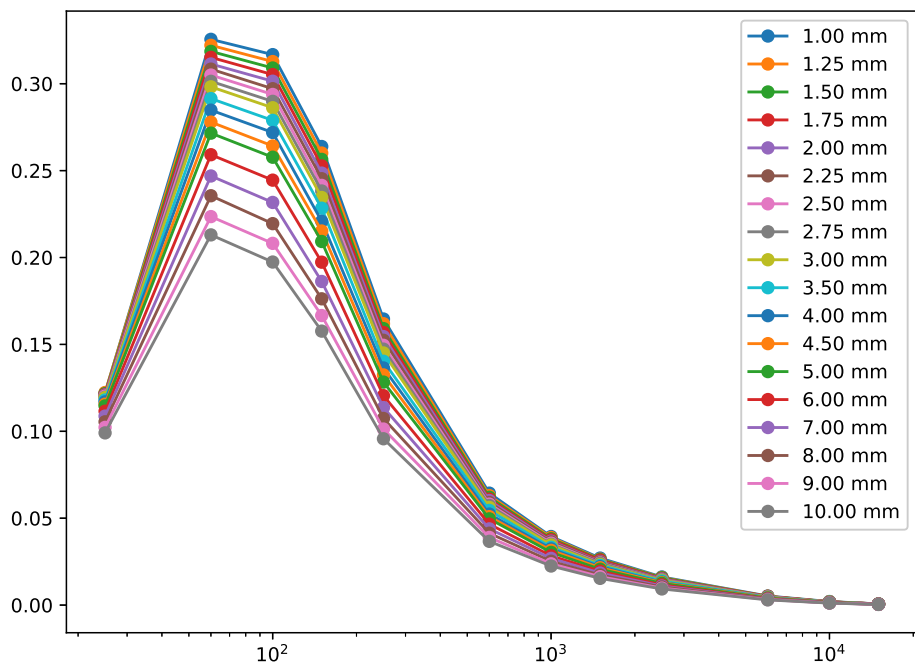


Figure 15: Full peak efficiency curves at various distances

I used the virtual point detector approximation to fit the distance dependence. The solid angle correction scales with r^{-2} but the sample-detector distance is not the actual sample-detection distance. The crystal sits behind the end cap and the effective detection point is not necessarily the front or middle of it. The correction factor according to [11] is $\propto \frac{1}{(r+r_0)^2}$, where r_0 is the effective detection distance inside the detector.

The r_0 distance can be easily acquired by plotting $N(r)^{-\frac{1}{2}} \propto \mu(r)^{-\frac{1}{2}}$, fitting it

with a line and finding its r axis intercept (as $r - r_0$ is 0 at r_0). Using this method I calculated the r_0 values for each energy for both photo and total efficiencies.

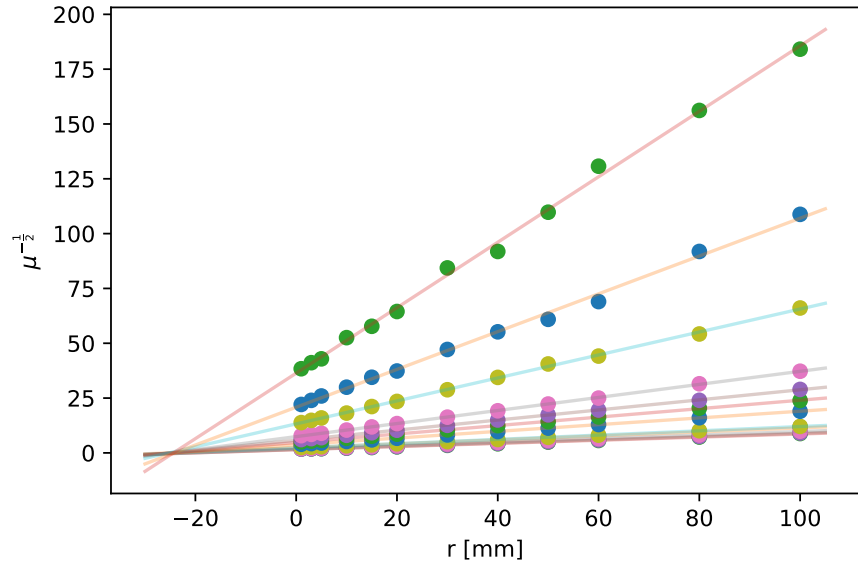


Figure 16: $\mu^{(P)^{-\frac{1}{2}}}$ plotted as a function of r for each energy with linear fit. The resulting lines intercept the r axis nearly at the same point. The interceptions are the r_0 values for the various energies

Plotting the resulting $r_0(E)$ values it is clear that they are energy dependent, Fig 17. The following empirical formula describes the dependence [11]:

$$r_0(E) = z_1(1 - e^{-z_2 E + z_3}),$$

where $z_{1,2,3}$ are parameters to fit. I have found that while this works for distances at $\approx 10\text{cm}$ order, it is not usable for small distances of a few mm. After all this is not that surprising given that this is a point detector estimation, the detector is not that point-like from a close distance. Based on the shape of the curve and the previous equation I ended up using

$$r'_0(E) = z'_1(1 + e^{-z'_2 E + z'_3})$$

for small distances and it seems to work. One could ask how to properly fit $r_0(E)$ for both cases, and as I later realized probably the correct answer is by not using the point detector assumption at all but properly calculating the solid angle subtended by the detector. After this there would probably still be an energy and maybe distance dependent r_0 , depending for example on the average detector depth over the detector solid angle. While further investigation sounds interesting, it is not part of my current work.

The plots on Fig 17 show an acceptable fit and the effective distances are comparable to the distance to the center of the detector at $\approx 5 + \frac{42}{2} = 26$ mm. The 25 keV point is ignored for both fits as it is an outlier, the cross section of photoelectric effect is smaller at low energies, resulting in a longer mean free path and a larger effective distance. Also there might be some difference at high energies but it is hard to tell because of the uncertainties present. This way some limits on the range of validity are given (or at least its lower limit is certainly known).

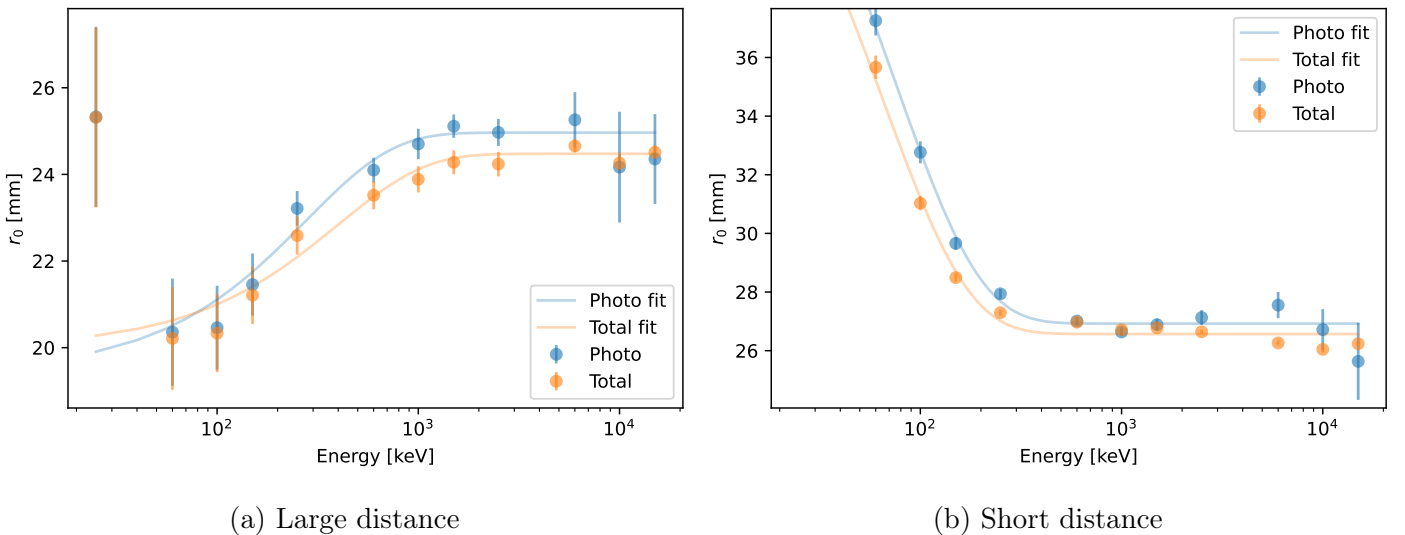


Figure 17: The $r_0(E)$ functions for photo and total efficiency distance dependence for small and large sample distances. The 25 keV point is an outlier on both plots, more noticeably at large distances. At small distances its value is $r_0(25\text{keV}) \approx 80$ mm.

The resulting distance dependence functions were used to refit the 5th order polynomial approximation, a single polynomial was fitted for all distance per photo/total type per run set (4 fits total). The fits were evaluated by comparing them to the simulated data efficiencies, the data/fit ratio is shown in Fig 18. The fits seem to do a good job between ≈ 100 keV and $\approx 6\text{MeV}$. At low energies the distance dependent error is expected, as previously mentioned. At large energies for photo efficiencies the error of r_0 was big, which could explain the noticeable "red" error. Also note that at $10+$ MeV the efficiency is of 10^{-4} order, so we are talking about only a few hundred hits, the error of efficiency simulation itself is non negligible. There seems to be a distance dependent error component for all energies in the large distance fits. This can be explained by the fact that the "large" distance goes from 1mm to 10cm so while the $\mu(r)^{-\frac{1}{2}}$ points seem to fall on a line from far away, the more densely packed small distance points could be distorting the linearity of the data. For small distances there is no such distance dependant error.

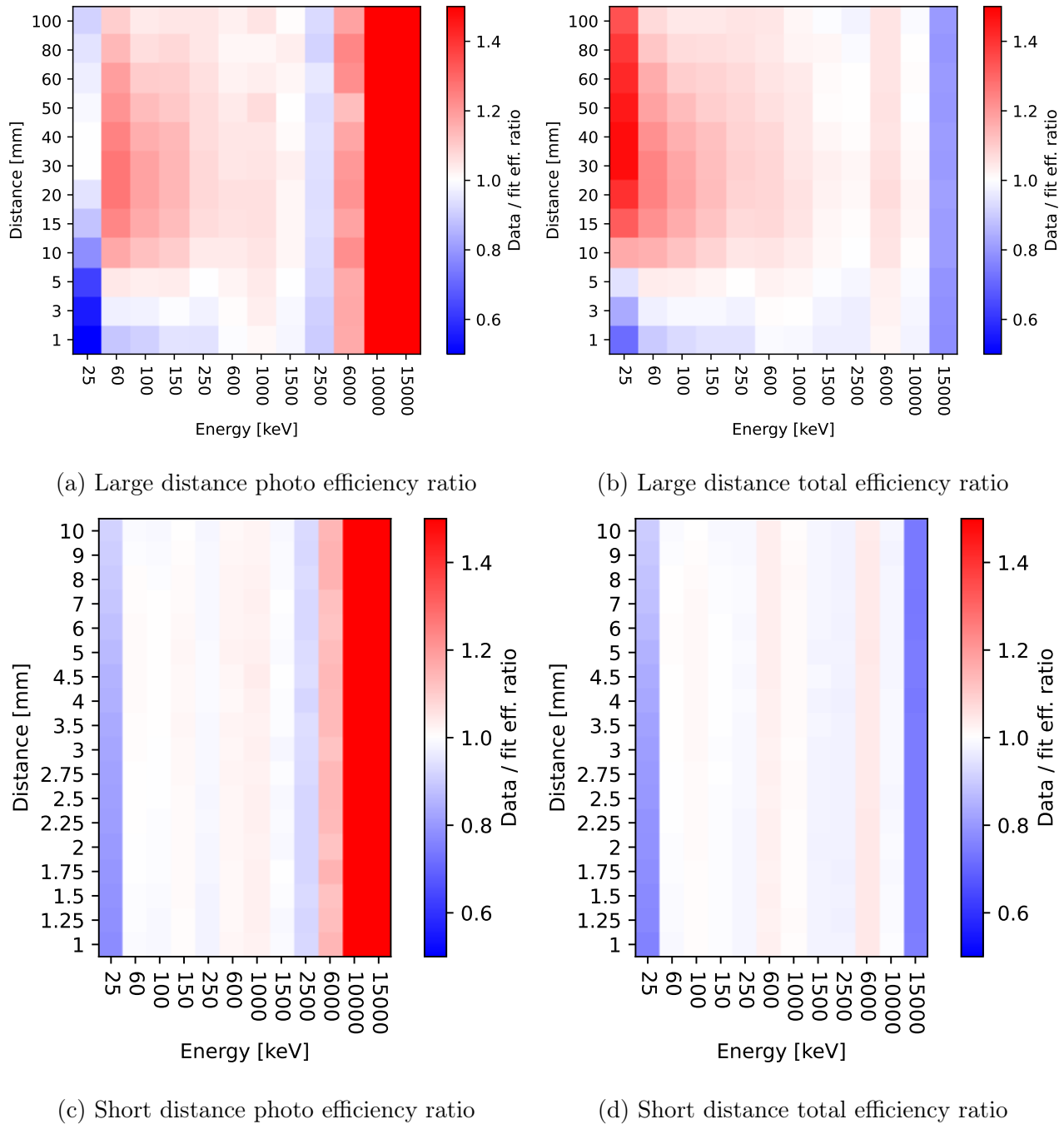


Figure 18: Ratio of efficiency data points per distance-energy dependent efficiency fit evaluated at simulation points for all 4 fits

4.2 Construction of matrices for ^{208}Tl

^{208}Tl β^- decays with 100% intensity into ^{208}Pb . After the initial β^- decay the daughter nucleus, ^{208}Pb is in an excited state, generating a gamma cascade while transitioning to its ground state. I created the correction matrices for this specific isotope because after the decay of ^{208}Tl the daughter nucleus cannot be in ground state and its first level's feeding factor is 0 too, so gamma cascades are guaranteed.

There are three main parts to constructing the correction matrices:

- constructing the transition probability matrix (from literature)
- constructing the efficiency matrices (from simulation)
- combining the two according to the formulas specified in Section 2.3 (done with python code)

4.2.1 Transition probability matrix

First of all I needed the energy levels of ^{208}Tl and then I had to acquire the transition probabilities from state j to i . I got the list of levels from [9] with the gamma intensity and feeding factors (summing up to 99.986%) of 17 levels (there are higher levels of course but as the feeding factors add up to almost the whole intensity with only 0.014% missing and it is within error of the sum, these are the levels playing a role in the phenomenon). Gamma intensity is the intensity (as a percentage) of a gamma transition happening, the same value we called ε in Section 2.3.1.

To get the transition probabilities I had to use the full intensities $I = I_\gamma(1+\alpha+\alpha_{IPF})$, not just the gamma intensity, as internal conversion and internal pair production should be taken into account too. To calculate this I needed the conversion coefficients, α for internal conversion and α_{IPF} for internal pair formation. The conversion coefficients specify the rate of internal conversion (and pair production) relative to gamma emission. These values were also given in [9], they were calculated using BrIcc [10] with the 'Frozen Orbitals' approximation.

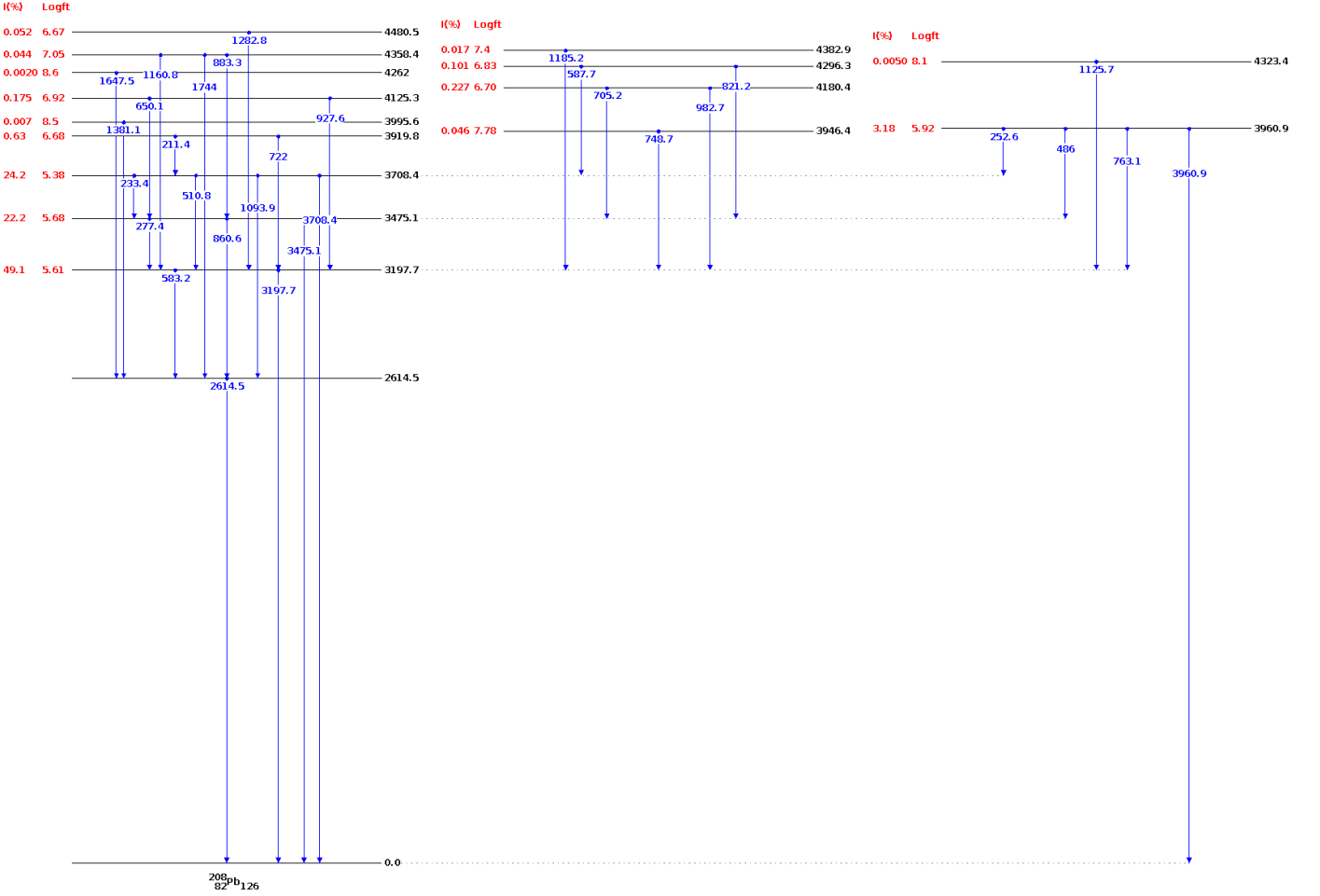


Figure 19: Decay scheme of ^{208}Tl [9]. Energy levels with feeding ratios and all possible transitions with their energies

Knowing the outgoing intensities from a level j , the ratio of transition probabilities is the same as the ratio of outgoing intensities, also $\sum_i X_{ij} = 1$, so $X_{ij} = \frac{I_{ij}}{\sum_i I_{ij}}$, this way of X_{ij} derivation was introduced to me through the work of Bodor, Á. Cs. [17]. After this using the conversion coefficients I could easily calculate $\underline{\underline{G}}$, $\underline{\underline{E}}$ and $\underline{\underline{W}}$.

$$\underline{\underline{G}} = \frac{1}{1 + \alpha + \alpha_{\text{IPF}}} \underline{\underline{X}}$$

$$\underline{\underline{E}} = \frac{\alpha}{1 + \alpha + \alpha_{\text{IPF}}} \underline{\underline{X}}$$

$$\underline{\underline{W}} = \frac{\alpha_{\text{IPF}}}{1 + \alpha + \alpha_{\text{IPF}}} \underline{\underline{X}}$$

	0	2614.529	3197.717	3475.088	3708.41
0					
2614.529	1				
3197.717	4.63E-05	0.999954			
3475.088	6.54E-05	0.559058	0.440876		
3708.41	7.73E-05	0.016615	0.962944	0.020363	
3919.78			0.394532		0.605468
3946.42			1		
3960.93	0.000472		0.583735	0.01543	0.400362
3995.6		1			
4125.28			0.714286	0.285714	
4180.38			0.903084	0.096916	
4262		1			
4296.28				0.405941	0.594059
4323.4			1		
4358.44		0.045455	0.25	0.704545	
4382.9			1		
4480.5			1		

Table 1: $\underline{\underline{X}}$ matrix for ^{208}Tl with level energies in keV

Matrix is transposed and zero elements to the right are not shown to fit onto page

I double checked my computations by calculating all ε from \underline{f} , $\underline{\underline{X}}$ and $\underline{\underline{G}}$ and verifying that it is indeed equal to I_γ . The maximum relative error was in 10^{-3} order, probably due to small errors from the not exact numbers amplifying, but this is still an acceptable error.

4.2.2 Corrected intensities

The efficiency matrices were calculated at 2 mm distance using the short distance fit created in Section 4.1.4. The $O_{1,2,3}$ matrices were calculated as described in 2.3 from $\underline{\underline{X}}$, $\underline{\underline{G}}$, \underline{f} and $\underline{\underline{H}}^{(P,T)}$. The resulting corrected relative intensities are listed in Appendix A.1, I will not detail their the exact values here. Instead I discuss the $\frac{O_1 O_2 O_3}{I_\gamma}$ ratios as these can be interpreted on their own without requiring the reader to cross check two large tables.

	0	2614.529	3197.717	3475.088	3708.41
0					
2614.529	0.752				
3197.717	1477.834	0.794			
3475.088	521.095	0.951	0.693		
3708.41	83.108	6.620	0.690	0.648	
3919.78	inf	inf	0.819	inf	0.569
3946.42	inf	inf	0.696		
3960.93	7.106	inf	0.760	0.699	0.569
3995.6	inf	0.863			
4125.28	inf	inf	0.712	0.655	
4180.38	inf	inf	0.700	0.655	
4262	inf	0.863			
4296.28	inf	inf	inf	0.658	0.569
4323.4	inf	inf	0.696		
4358.44	inf	1.854	0.797	0.655	
4382.9	inf	inf	0.696		
4480.5	inf	inf	0.696		

Table 2: Corrected / uncorrected intensity ratio at 2 mm source distance. Inf is infinity for transitions with no direct transition, $I_\gamma = 0$, these can only be detected with coincidences (but most of them only with small corrected intensities)

Matrix is transposed and zero elements to the right are not shown to fit onto page

Investigating the ratio of corrected and uncorrected intensities the most obvious difference is the number of new transitions, written as infinite ratios. The not allowed transitions can be detected due to summing-in. Unfortunately most of these transitions have a $\approx 10^{-8}$ intensity, with some exceptions, the maximal intensity is of the 3960 keV \rightarrow 2614 keV transition with a corrected intensity of 4.79×10^{-5} , which is still pretty low compared to the 0.01 intensity of the 2614 keV transition. It could make it a detectable peak in the measurement if it weren't at such a low energy, as we will see later it's lost in the Compton background's still too high noise, unlike the 3708 keV transition which only has a 1.7×10^{-5} intensity but at 3.7MeV the Compton noise is orders of magnitude smaller.

Next are the transitions with large ratios, the same thing is happening as with the previous category, but here there are direct transitions too. As an example for 3197 keV \rightarrow 0 keV, as X_{13} is only 4.6×10^{-5} while $X_{23} = 0.999954$ and $X_{12} = 1$, the probability

of 2 coincidental detections from this level is $\approx \mu^{(P)2}$ while the single step probability is $\approx 4.6 \times 10^{-5} \mu^{(P)}$ so the expected ratio is $\approx 2000\mu^{(P)}$ ⁷.

These are the transitions that make the most striking difference with the correction, low direct transition probability from j to i but i is accessible from j through a few high probability transitions. As a rule of thumb this is the case as long as $g_{\text{rare}} \ll g_{\text{freq}}^l \mu^{l-1}$, where g_{rare} is the improbable direct gamma transition probability, g_{freq} is the (characteristic) probable one and μ is a characteristic efficiency for the whole l step long coincidence chain.

The remainder of the matrix are the elements smaller than one, these are due to the effect of summing-out, as coincidences sum-in they have to sum-out of somewhere lowering the intensity, plus there is the summing-out of partial detections (with the efficiency of $\mu^{(T)} - \mu^{(P)}$).

⁷Of course $\mu^{(P)}$ is not constant, but about the same order for both transitions, also \underline{X} is not the gamma transition probability, etc. This is just a crude approximation to show this is the expected result

5 Applying to ^{208}Tl measurement

5.1 Measurement

To apply the correction and test my predictions on experimental data I needed the results of a measurement done with the detector. I got the spectrum of a mineral deposit sample, precipitated from thermal water onto pipes in Bükk, Hungary in ≈ 1995 . I also got a background radiation measurement (without any sample) that was run for 5 days at the time. The known parameters of the measurements are shown in Table 3.

	Measurement	Background
Sample	Mineral deposit	-
Sample distance	$\approx 2\text{mm}$	-
Duration	1 day	5 days
Gain	4	4
Threshold	40	40
Preamplifier	0.7	1

Table 3: Detector settings for the measurements

5.2 Fitting peaks of experimental data

The spectra were in the form of two .mac file, basically just the measurement time and a list of hit counts (per channel). I had to analyze the data, find the appropriate peaks, calculate their area (sum hit count) and of course subtract the background. I used a gamma spectrum analyzer program called Spill (version 6.1) and in the case of double or multiple peaks overlapping I used python to fit all of them at once (something Spill is not able to do yet, unfortunately).

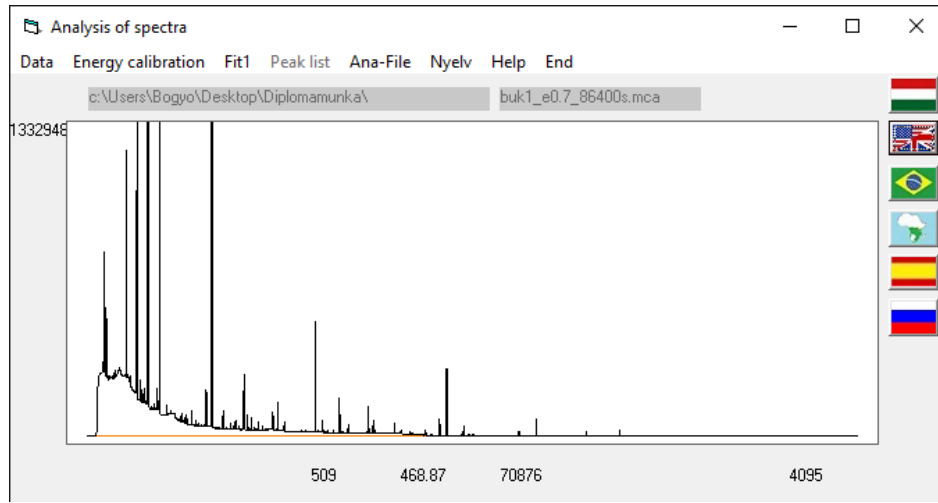


Figure 20: The spectrum of the measurement with the sample shown in Spill

The calibration section of the file was not properly filled, so first of all I had to identify a few peaks of the uranium chain to be able to convert from channel number to energy. The calibration used a 2nd degree fit from 3 points (the energy-channel relation is almost linear but not exactly) and in most cases the energy of the read peaks was accurate within a 1keV error.

For the case of merged together but still distinctive peaks I had to work outside of Spill. I calculated their area in python the following way:

1. I fitted them with a linear baseline plus the sum of peak number of gaussians
2. Removed the peak of interest from the fit
3. Subtracted the resulting fitted peaks with the exception of the target peak from the data
4. Summed the difference around the target peak

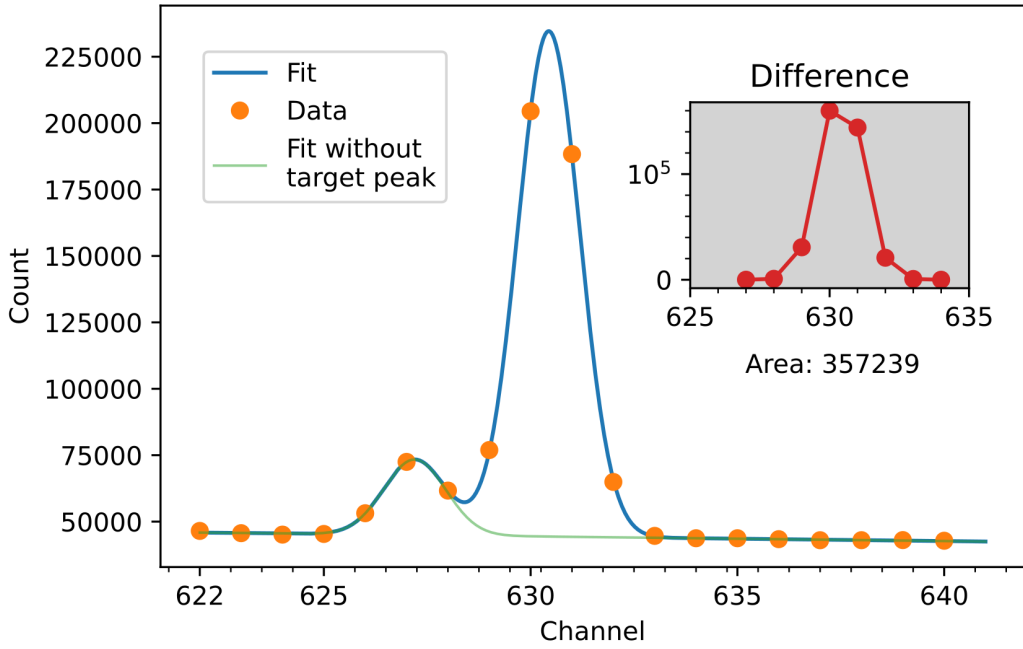


Figure 21: The multiple peak fitting process shown at the 583 keV gamma peak merged with the 580 keV peak of ^{214}Pb . The green curve, the multigauss fit with the target peak removed from it, is subtracted from the data. This results in the red peak (shown in the inset) being the approximated target peak, whose area (sum of counts) is the required value

This method has a varying degree of reliability depending on the closeness of the peaks, the height of the target peak, the linearity of the baseline, the proximity of larger peaks (with significant contribution even 5-10 channels away from their peak), the possibility of other "hidden" peaks and various other factors, so regardless of the error of the actual fit (which was often insignificant) I have found some cases more unreliable and just estimated a larger error by eye.

∞

Transition keV → keV	E_γ [keV]	Area [hits]	Error [hits]	Background [hits]	Notes
3960.9→3708.4	252.5	9796	3000	-	The peak was extremely small and hard to fit so it has a huge error (error of fit + overestimation by eye, the fit error alone seemed unrealistically small)
3475.1→3197.7	277.4	47678	2800	-	Double peak
3708.4→3197.7	510.7	161744	1210	648.4	"Single" peak but right on 511keV with positron background
3197.7→2614.5	583.2	357239	6130	56	Double peak (with 2 other in the close vicinity, fitted quadruple gaussian)
3960.9→3197.7	763.2	-	-	-	Failed to calculate, 768keV ^{214}Bi peak is too close with high intensity
3475.1→2614.5	860.6	40668	792	-	
3708.4→2614.5	1093.9	5280	3000	-	Double peak
2614.5→0	2614.5	97847	350	55	
3197.7→0	3197	3331.8	64	No data	Peak slightly off
3475.1→0	3475	337.5	25	No data	Peak seems to be off about 10 keV
3708.4→0	3708	73.8	15	No data	Peak seems to be off about 12 keV

Table 4: Peak data from measurement. Peaks without "Double peak" notes are fitted using Spill, peaks with "Double peak" fitted in python. Area errors are estimated by Spill (where relevant, $\sqrt{B_{\text{peak}}} + \sqrt{B_{\text{compton}}}$) + error of fit (in python, where relevant) + error overestimation by eye if necessary (fit error doesn't cover the whole real error) + error of background (Spill). Transitions with no background specified did not have a discernible peak in the background spectrum, for these background correction was neglected

As seen in Table 5.2, most peaks had some kind of problems. Out of the 31 possible transitions only 11 peaks were discernible, the 763 keV peak was still impossible to properly estimate and the 252 keV peak was barely measurable. The 860 keV and 2614 keV ones were the only two clear, single peaks.

The $>3\text{MeV}$ peaks were offset from their expected position but the offset seemed to be consistent, so I assumed they are the peaks I was looking for. A possible reason for this could be that these peaks were at the very end of the measured energy range and the last calibration point was set to 2614 keV, so errors in the channel number - energy function are possible at this range. The last three peaks, while expected to be extremely small without coincidence correction ($\varepsilon_{1i} \approx 2 \times 10^{-5}$), are the ones receiving the largest corrections. The 3919 keV peak was unfortunately already out of the measurement range although it would have been interesting to see whether it is there as there is no direct transition to ground state from 3919 keV, so all of it would be coincidence.

5.3 Activity correction

5.3.1 Activity at 2mm distance correction

I have calculated the activity without coincidence correction ($A_0 = \frac{B}{\varepsilon \mu(P)t}$) and using the coincidence corrected equation in Section 2.3.4 using the distance and energy dependent efficiency approximation (fitted for the small distance run set) detailed in Section 4.1.4 at 2 mm distance.

I calculated the activity for each peak independently, with their error originating from the background-corrected peak area error. The error of the efficiency fit was not propagated through the calculation. I also calculated the deviation of activities and the average activity of all peaks weighted with inverse variance.

$$\bar{A} = \frac{\sum_i A_i \frac{1}{\sigma_i^2}}{\sum_i \frac{1}{\sigma_i^2}}$$

E_{peak}	[keV]	252.5	277.4	510.7	583.2	860.6	1093.9	2614.5	3197.7	3475.1	3708.4
A_0	[Bq]	93.4	59.6	117.1	79.9	91.6	428.1	72.5	76693.3	22988.4	4101.7
A	[Bq]	164.1	86.0	169.6	100.7	96.3	64.7	96.4	51.9	44.1	49.4
σ_{A_0}	[Bq]	28.6	3.5	0.9	1.4	1.8	243.2	0.3	1473.2	1600.7	699.2
σ_A	[Bq]	50.3	5.1	1.3	1.7	1.9	36.7	0.3	1.0	3.1	8.4

Table 5: Calculated activities and their error
 A_0 uncorrected and A with coincidence correction

As seen in Table 5 and on Fig 22 the resulting activities are not exactly a perfect constant value. Both the corrected (A) and uncorrected (A_0) values have problems. While the 1093 keV peak is quite an outlier in A_0 the correction seems to put it slightly under the average activity value (although it is within error). The 252 and 510 keV peaks seem to get a bit overcorrected too. As a result the uncorrected fit might seem to be better, apart from the 1093 keV point (although it has a large error), but let's not forget about the 3 high energy peaks. All 3 peaks over 3MeV give an unrealistically big activity result using the uncorrected method as their intensity is extremely low. But 2 and 3 step coincidence are quite likely for these peaks as was seen, e.g. both $3197 \rightarrow 2614$ and $2614 \rightarrow 0$ keV are high intensity transitions.

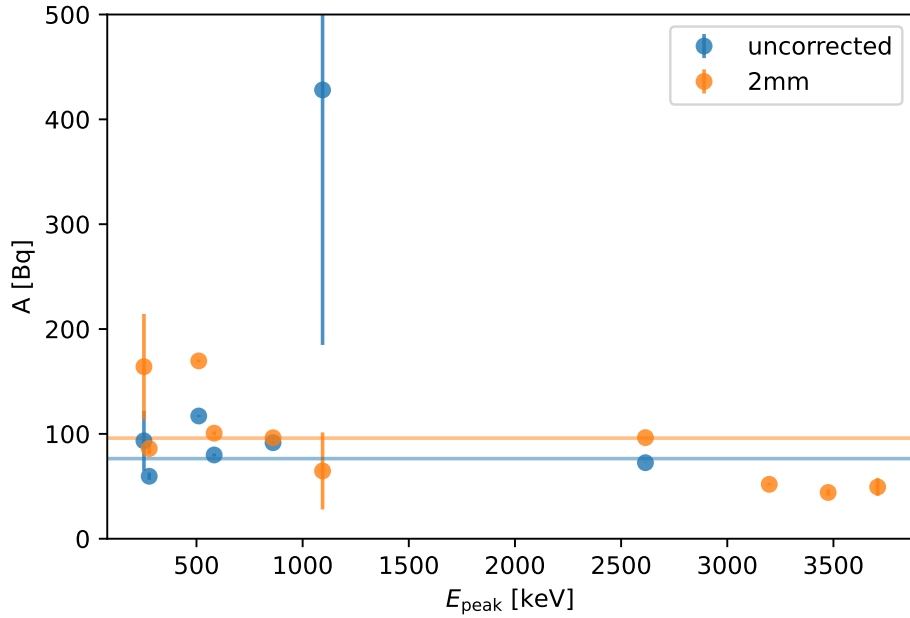


Figure 22: Activity calculated from background-corrected peak areas using the uncorrected and coincidence corrected method at 2 mm sample distance. Horizontal lines are weighted average activity.
Note that the last 3 points of the uncorrected method are ignored as they are in 10 000 Bq order

All together the 3 high energy peak adjustments nicely show that the correction calculations worked, also the 1093 keV peak was somewhat corrected, and only the 252 and 510 keV peaks seem to be slightly misplaced, although the 252 keV one has a rather large error so its not that far away.

The corrected average activity of 96.0 ± 7.6 Bq is $\approx 25\%$ higher than the uncorrected 76.4 ± 5 Bq⁸.

5.3.2 Activity over distance

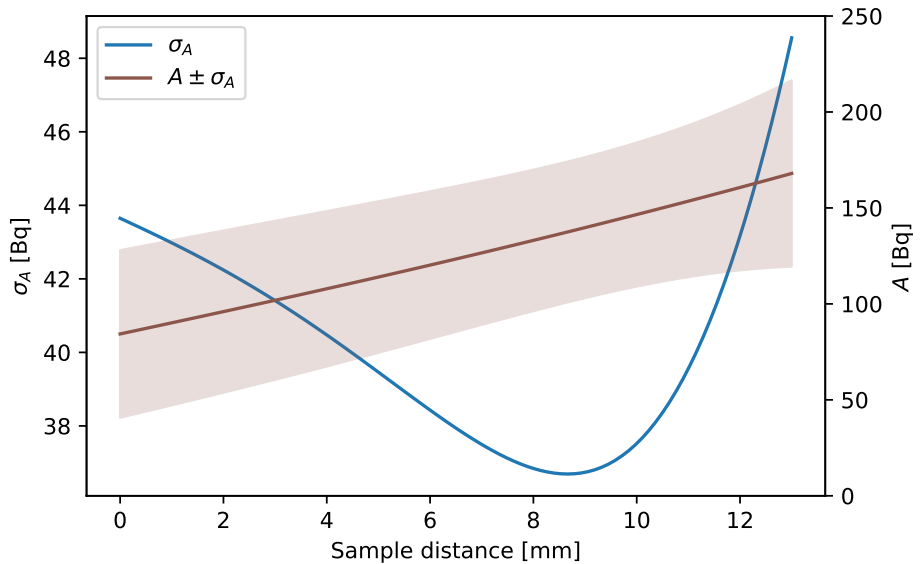


Figure 23: Standard deviation of corrected activities at each distance and average weighted activity \pm standard deviation. Here the error of various peak areas was not taken into account for the standard deviation estimation

As the exact location of the sample is not known (only that it was directly on the detector, then the width of the container wall + half width of the sample was estimated to be about 2 mm) I decide to check at what distance would the calculated activities agree the most.

I used the standard deviation of the activities (without taking the errors into account). The resulting minimum deviation distance was found to be ≈ 8.7 mm with an average activity of 137 Bq. While the activities are certainly closer, as visible on

⁸Error calculated by fitting a constant function using scipy's curve_fit with sigma= σ_A

Fig 24, the sample container was definitely not 8 mm thick nor was the sample 1.5 cm wide, so the actual precise position cannot be fitted.

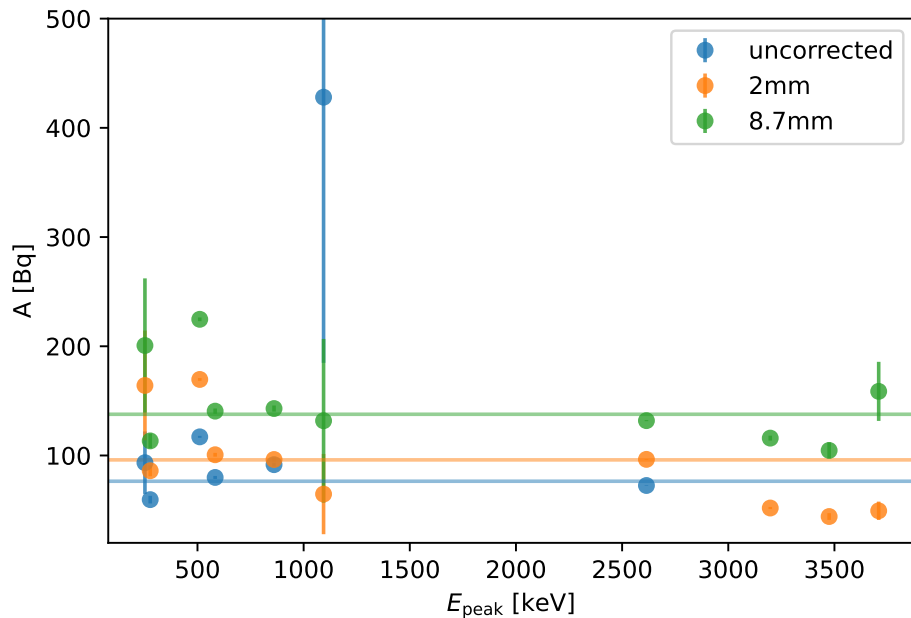


Figure 24: Calculated activities for all peaks, uncorrected, and coincidence corrected at 2 mm and 8.7 mm

6 Summary

I investigated the coincidence correction in the HPGe detector of Department of Atomic Physics, ELTE. I simulated the detector using Geant4 based on the technical specification, outer measurements and a technical drawing. The created simulation besides having the monoenergetic mode I used for distance and energy dependent efficiency simulation, has other modes for various further investigations including direct ^{238}U decay simulation (using RadioActiveDecayProcess or energy distribution based single primary gamma emissions) or investigation of self-absorption via the simulation of the sample and sample holder.

I calculated the photopeak and total efficiencies at various distances over a high range of energies using the simulation and gave a 2 dimensional fit of them for both short and long sample distances. I have shown that the fits give a good approximation of the efficiencies in the 100keV-5MeV range with some error present in the high energy ($>5\text{MeV}$) and a distance dependent error present in the low energy ($<100 \text{ keV}$) region, for which I gave an idea for a possible correction.

I have collected the transition probabilities, internal conversion and pair production ratios and feeding factors of ^{208}Tl β^- decay from literature and using these and the fitted efficiencies constructed the necessary coincidence correction matrices and coincidence corrected intensities of its gamma transitions using Semkow's matrix formalism. I have analyzed the resulting corrected intensity matrix compared to the uncorrected gamma intensities and shown the effects and mechanisms of summing-in and summing-out.

I analysed a previously measured environmental sample's gamma spectrum, identified and measured the peaks of ^{208}Tl using the Spill 6.1 spectrum analyser program and my own multi-Gaussian fitting python code. I determined the corrected and uncorrected activities for each peak, discussed the differences and shown that the coincidence corrected results show a better agreement, especially at the high energy $>3\text{MeV}$ peaks, whose correction factor reached even $\times 1400$ correction. I determined the averaged activity of the peaks and found that the correction introduced a 25% increase in the estimated activity.

Additionally I also investigated the sample distance dependence of the calculated average activity and its (unweighted) standard deviation to find out that the precise

fitting of exact sample distance is not possible due to the large uncertainties as the minimal deviation was found at a distance far greater than the estimated sample distance.

The implemented coincidence correction process (written in python and C++ (Geant4)) can be easily applied to experimental data, for other isotopes too, once the proper gamma intensities, conversion factors and feeding factors are collected (e.g. from NuDat2) and the peak areas are determined (e.g. using Spill).

While I have investigated many things there are still quite a few assumptions made and phenomena ignored at most steps of the process, leaving room for plenty of future improvement and follow-up research.

For the simulation: the dead layer of the Ge crystal could be considered, this would effect the efficiency of the detector, especially in the low energy range [14], as photons are not detected in this layer. Also sample self-absorption plays a big role at low energies as shown on Fig 1, the simulation was made ready for the analysis of this effect but I have not carried it out yet. The energy dependent efficiency decreases would lead to energy and μ order dependant correction changes. Also the source was assumed to be a point source, this approximation could be left behind and a 3D source could be used, the simulation is able to do this too through the Geant General Point Source by setting a source volume or it could be analytically calculated by integrating the point source over the sample volume. Also in 3D samples the possibility of inhomogeneous activity distribution arises.

Also for verifying the simulation the various efficiency results could be compared to new calibration measurements, the simulation could be fine tuned to precisely mirror the real life detector. For this an X-ray image or CT scan of the detector could greatly help for even more precise geometry modelling[5]. Also the ^{238}U simulation could be compared to the actual measured spectrum. For comparison to experimental data the simulation of readout would also be needed.

For the measurement analysis: peaks of other isotopes could also be measured and their activities calculated after the needed inputs ($\underline{\underline{X}}$, \underline{f} , $\underline{\alpha}$) are gathered from literature. The weighted average of each isotope could be compared to each other to decide whether the sample is truly in radioactive equilibrium or just to get more measurement points for a better, more precise activity calculation.

References

- [1] <https://github.com/Balazzs/HPGECalorimeter>
- [2] Thomas M. Semkow, Ghazala Mehmood, Pravin P. Parekh and Mark Virgil
Coincidence summing in gamma-ray spectroscopy
Nuclear Instruments and Methods in Physics Research. A290 437-444. (1990)
- [3] S. Agostinelli *et al.* [GEANT4 Collaboration]
GEANT4: A Simulation toolkit
Nuclear Instruments and Methods, Vol. 506, No 3., 250-303. (2003)
- [4] M. Ahmed, M. Gouda, M. Badawi, S. Nafee, E. El-Mallah
Computation of the full energy peak efficiency of an hpge detector using a new compact simulation analytical approach for spherical sources
Journal of Engineering Science and Technology, Vol. 8, No. 5, 623-638. (2013)
- [5] Szentmiklósi, László & Belgya, Tamas & Maróti, Boglarka & Kis, Zoltan.
Characterization of HPGe gamma spectrometers by geant4 Monte Carlo simulations
Journal of Radioanalytical and Nuclear Chemistry, Vol. 300, No. 2, 553-558. (2014)
- [6] Klein, O. & Nishina, Y.
The Scattering of Light by Free Electrons according to Dirac's New Relativistic Dynamics
Nature Vol. 122, 398–399. (1928)
- [7] Molnár, G.L.; Zs. Révay; T. Belgya.
Wide Energy Range Efficiency Calibration Method for Ge Detectors
Nuclear Instruments and Methods in Physics Research, Section A: Accelerators, Spectrometers, Detectors and Associated Equipment, Vol. 489, No. 1–3, 140–59. (2002)
- [8] Elekes, Z.; Belgya, T.; Molnár, G. L.; Kiss, Á Z.; Csatlós, M.; Gulyás, J.; Krasznahorkay, A.; Máté, Z.
Absolute full-energy peak efficiency calibration of a Clover-BGO detector system
Nuclear Instruments and Methods in Physics Research, Section A: Accelerators, Spectrometers, Detectors and Associated Equipment. Vol, Vol. 503, No. 3, 580-588. (2003)
- [9] Martin, M. J.
Nuclear Data Sheets for A = 208
Nuclear Data Sheets, Vol 108, No. 8, 1583–1806. (2007)

- [10] T. Kibédi, T.W. Burrows, M.B. Trzhaskovskaya, P.M. Davidson, C.W. Nestor, Jr.
Evaluation of theoretical conversion coefficients using BrIcc
 Nuclear Instruments and Methods, Vol. 589, 202-229. (2008)
- [11] Notea, A.
The Ge(Li) spectrometer as a point detector
 Nuclear Instruments and Methods, Vol. 91, No. 3, 513–515. (1971)
- [12] Andreev, D S, Erokhina, K I, Zvonov, V S, and Lemberg, I Kh.
Consideration of cascade transitions in determining the absolute yield of gamma rays
 Prib. Tekh. Eksp., Vol 15, No. 5, 63-65. (1972)
- [13] D. S. Andreev, G. M. Gusinsky, A. P. Grinberg, K. I. Erokhina, R. K. Zhirgulevichus, V. S. Ivanov, I. Kh. Lemberg, A. A. Pasternak
Life Times of the 0.872, 1.106, 1.336 MeV Levels in ^{69}Ga and the 0.910 and 1.395 MeV Levels in ^{71}Ga
 Program and Theses, Proc. 23rd Ann. Conf. Nucl. Spectrosc. Struct. At. Nuclei, p. 360 (1973)
- [14] McCallum, Graham J., és Graeme E. Coote.
Influence of Source-Detector Distance on Relative Intensity and Angular Correlation Measurements with Ge(Li) Spectrometers
 Nuclear Instruments and Methods, Vol. 130, No. 1, 189–97. (1975)
- [15] Sima, O.
Applications of Monte Carlo Calculations to Gamma-Spectrometric Measurements of Environmental Samples
 Applied Radiation and Isotopes, Vol. 47, No. 9–10, 919–23. (1996)
- [16] Horváth, Á.
A kaszkád gamma-fotonok összeadódásának jelensége a gamma-spektroszkópiában és ennek numerikus kezelése
<http://atomfizika.elte.hu/akos/orak/mkm/coszu.pdf>
- [17] Bodor, Á. Cs.
Koincidencia-korrekciónak számítása gamma-spektroszkópiában
 32. OTDK, Fizika, Földtudományok és Matematika Szekció, Természettes radioaktivitás Tagozat (2015)
<http://atomfizika.elte.hu/akos/tezisek/tdk/bodoraron.pdf>
- [18] ^{238}U és a ^{232}Th bomlási sorának 0,001 relatív intenzitás feletti gamma-bomlásai
<http://atomfizika.elte.hu/akos/orak/trad/gammatabla.html>

A Appendix

A.1 Coincidence corrected intensities

	0	2614.529	3197.717	3475.088	3708.41
0					
2614.529	1.17E-02				
3197.717	7.43E-04	4.11E-02			
3475.088	8.85E-05	4.89E-03	6.41E-03		
3708.41	1.73E-05	9.45E-04	1.10E-02	3.39E-04	
3919.78	1.31E-07	7.24E-06	9.56E-05	4.41E-07	1.90E-04
3946.42	2.02E-08	1.12E-06	1.51E-05		
3960.93	1.01E-06	4.79E-05	6.30E-04	2.55E-05	6.91E-04
3995.6	2.98E-08	1.65E-06			
4125.28	5.53E-08	3.05E-06	3.42E-05	1.78E-05	
4180.38	7.39E-08	4.08E-06	5.23E-05	7.20E-06	
4262	7.36E-09	4.07E-07			
4296.28	9.30E-09	5.12E-07	2.05E-06	1.16E-05	2.06E-05
4323.4	1.51E-09	8.33E-08	1.13E-06		
4358.44	1.51E-08	8.34E-07	2.76E-06	8.16E-06	
4382.9	4.90E-09	2.71E-07	3.66E-06		
4480.5	1.40E-08	7.76E-07	1.05E-05		

Table 6: $O_1O_2O_3$, coincidence corrected intensities for ^{208}Tl using the efficiency from the distance and energy dependent fit of short run set at 2 mm sample distance. Magnitude based coloring for readability. The matrix is transposed and zeros are cropped to fit onto page.

A.2 Energy and distance dependent efficiencies

	Energy [keV]												
	25	60	100	150	250	600	1000	1500	2500	6000	10000	15000	
Distance [mm]	1	0.122061	0.325539	0.316743	0.263868	0.164612	0.064416	0.039455	0.027056	0.016194	0.005237	0.00205	0.000679
	3	0.119402	0.298238	0.286081	0.234796	0.144741	0.055966	0.034568	0.023468	0.014057	0.004541	0.001742	0.000591
	5	0.114518	0.271878	0.25777	0.209084	0.12792	0.049459	0.030323	0.02069	0.012483	0.003933	0.001484	0.000544
	10	0.09883	0.213197	0.197744	0.157463	0.095739	0.036792	0.022459	0.01546	0.009231	0.003032	0.001114	0.000362
	15	0.082217	0.166012	0.152187	0.120752	0.073802	0.028398	0.017301	0.011855	0.007134	0.002238	0.000841	0.0003
	20	0.067285	0.130915	0.119149	0.094785	0.057952	0.022415	0.013682	0.009341	0.005601	0.001815	0.000717	0.000241
	30	0.04536	0.084241	0.076966	0.061632	0.038159	0.014811	0.009089	0.006317	0.003763	0.001206	0.00045	0.000141
	40	0.031486	0.057649	0.052798	0.043126	0.02675	0.010554	0.00647	0.004434	0.002711	0.000844	0.000328	0.000119
	50	0.02281	0.041237	0.038148	0.031105	0.019889	0.007831	0.004936	0.003314	0.002014	0.000608	0.00027	0.000083
	60	0.01712	0.031114	0.028473	0.023671	0.01524	0.006	0.003721	0.002616	0.001601	0.000513	0.00021	5.85E-05
	80	0.01073	0.019111	0.017757	0.014994	0.009776	0.003885	0.002402	0.001738	0.001007	0.00034	0.000119	0.000041
	100	0.007178	0.012811	0.012107	0.010232	0.006845	0.002768	0.001751	0.001194	0.000721	0.000229	8.45E-05	2.95E-05

Table 7: Photopeak efficiency of long distance runs over various energies and distances. For more see Section 4.1.1 and 4.1.4

Distance [mm]	Energy [keV]												
	25	60	100	150	250	600	1000	1500	2500	6000	10000	15000	
67	1	0.122696	0.343073	0.352879	0.324142	0.273867	0.216686	0.187851	0.166385	0.145582	0.12693	0.128263	0.13304
	3	0.120027	0.312099	0.315047	0.286065	0.239389	0.187988	0.16381	0.144675	0.125452	0.109868	0.110788	0.115136
	5	0.115111	0.283193	0.282185	0.253196	0.21111	0.1659	0.14383	0.127602	0.110479	0.09606	0.097081	0.100991
	10	0.099292	0.220806	0.214829	0.189715	0.157666	0.123191	0.106899	0.095022	0.082257	0.071578	0.071993	0.075246
	15	0.082592	0.171648	0.165022	0.14524	0.120869	0.095278	0.082527	0.0726	0.063109	0.054956	0.055596	0.057479
	20	0.067584	0.134966	0.128932	0.113961	0.09479	0.074818	0.065117	0.057645	0.050184	0.043682	0.043948	0.045723
	30	0.045533	0.086788	0.083146	0.07372	0.062389	0.049477	0.042979	0.038529	0.033499	0.028935	0.029026	0.030085
	40	0.031614	0.059397	0.057174	0.05147	0.043499	0.035052	0.030517	0.02713	0.023627	0.020528	0.020657	0.021572
	50	0.0229	0.042493	0.041321	0.037056	0.032168	0.02577	0.022803	0.020148	0.017698	0.015445	0.015312	0.015995
	60	0.017186	0.032054	0.030817	0.028293	0.024601	0.019802	0.017643	0.015668	0.013747	0.011949	0.011967	0.012483
	80	0.010768	0.019708	0.019273	0.017907	0.015694	0.0128	0.011323	0.010314	0.008879	0.007811	0.007812	0.008091
	100	0.007211	0.013219	0.013138	0.01223	0.010952	0.009017	0.007923	0.007104	0.00618	0.005495	0.005427	0.005739

Table 8: Total efficiency of long distance runs over various energies and distances. For more see Section 4.1.1 and 4.1.4

Distance [mm]	Energy [keV]											
	25	60	100	150	250	600	1000	1500	2500	6000	10000	15000
1	0.122061	0.325539	0.316743	0.263868	0.164612	0.064416	0.039455	0.027056	0.016194	0.005237	0.00205	0.000679
1.25	0.122303	0.322107	0.312762	0.260111	0.161915	0.062988	0.038914	0.02644	0.015887	0.005076	0.001955	0.000666
1.5	0.121679	0.318604	0.309048	0.256449	0.159103	0.062042	0.038185	0.026233	0.015724	0.004954	0.001892	0.00068
1.75	0.121218	0.315163	0.305257	0.25271	0.156854	0.060978	0.037603	0.025874	0.015317	0.004985	0.001873	0.000668
2	0.120944	0.311355	0.301441	0.24857	0.154502	0.060163	0.036807	0.025077	0.015036	0.00476	0.001848	0.000635
2.25	0.120628	0.308384	0.297133	0.245337	0.152354	0.059048	0.036334	0.024797	0.014769	0.004764	0.001841	0.000614
2.5	0.120295	0.304992	0.293821	0.241494	0.149474	0.058093	0.035626	0.024286	0.014546	0.004707	0.001767	0.000602
2.75	0.119584	0.301381	0.289849	0.238279	0.147261	0.057299	0.034975	0.024047	0.014411	0.004618	0.001735	0.000595
3	0.119363	0.298215	0.286188	0.234545	0.145073	0.056178	0.03456	0.023385	0.014236	0.004452	0.001761	0.000571
3.5	0.117995	0.291445	0.278914	0.228367	0.140297	0.054467	0.033246	0.022839	0.013832	0.004375	0.001631	0.000582
4	0.116927	0.284801	0.271934	0.220841	0.136448	0.052377	0.032338	0.022129	0.013162	0.004239	0.001638	0.000526
4.5	0.115603	0.277921	0.264192	0.215246	0.13244	0.050891	0.031496	0.021497	0.012953	0.004114	0.001577	0.00055
5	0.114614	0.271562	0.257704	0.209223	0.128319	0.049629	0.030351	0.020653	0.01252	0.003963	0.001547	0.000516
6	0.111543	0.259154	0.244519	0.197318	0.120509	0.046547	0.02838	0.019496	0.011655	0.003683	0.001438	0.000458
7	0.10875	0.246918	0.231693	0.186212	0.113652	0.043864	0.026891	0.018458	0.010998	0.003482	0.001374	0.000459
8	0.105459	0.235544	0.219493	0.176238	0.107373	0.041358	0.025229	0.017296	0.010434	0.003365	0.001247	0.000454
9	0.102256	0.223543	0.208141	0.166619	0.101297	0.038948	0.023763	0.016363	0.009782	0.003183	0.001176	0.000413
10	0.099095	0.213019	0.1974	0.157647	0.09571	0.036687	0.022488	0.015386	0.009296	0.003	0.00115	0.000366

Table 9: Photopeak efficiency of short distance runs over various energies and distances. For more see Section 4.1.1 and 4.1.4

Note that while the colors show that energy dependence is stronger the data is still distance dependent

		Energy [keV]											
		25	60	100	150	250	600	1000	1500	2500	6000	10000	15000
$\frac{L_G}{L_\odot}$	1	0.122696	0.343073	0.352879	0.324142	0.273867	0.216686	0.187851	0.166385	0.145582	0.12693	0.128263	0.13304
	1.25	0.122937	0.339025	0.347601	0.319446	0.269191	0.211938	0.184896	0.163429	0.142077	0.124699	0.12565	0.130331
	1.5	0.122354	0.33494	0.342827	0.313946	0.264406	0.208655	0.181281	0.160843	0.14001	0.122323	0.123238	0.127949
	1.75	0.121868	0.33097	0.338123	0.308827	0.260389	0.204805	0.177788	0.157999	0.137363	0.120097	0.120708	0.125792
	2	0.121579	0.326802	0.333564	0.303714	0.255851	0.201768	0.175008	0.154675	0.135127	0.117878	0.119092	0.123287
	2.25	0.121275	0.323309	0.328382	0.299358	0.251566	0.198016	0.171958	0.15239	0.133089	0.115979	0.116867	0.121224
	2.5	0.120925	0.3194	0.324067	0.294311	0.247901	0.194409	0.169225	0.149985	0.130612	0.113617	0.114201	0.118999
	2.75	0.120229	0.315522	0.319629	0.290097	0.243697	0.191376	0.166262	0.147317	0.128194	0.111733	0.112546	0.116963
	3	0.119982	0.312099	0.315119	0.285256	0.239911	0.187855	0.163266	0.14486	0.126219	0.109742	0.110701	0.115142
	3.5	0.118609	0.304605	0.306815	0.277233	0.232042	0.181862	0.158382	0.140696	0.122245	0.106187	0.107175	0.111355
	4	0.117518	0.297184	0.298322	0.26832	0.225178	0.175948	0.152997	0.135554	0.117788	0.102915	0.103721	0.107557
	4.5	0.116188	0.289643	0.289543	0.261133	0.217928	0.171113	0.148294	0.13197	0.114555	0.099418	0.100015	0.104247
	5	0.115119	0.283104	0.282099	0.253559	0.211269	0.165824	0.143501	0.127161	0.11102	0.096658	0.096643	0.1009
	6	0.112111	0.26972	0.267095	0.23849	0.198571	0.155872	0.134912	0.119799	0.104	0.090439	0.091101	0.094639
	7	0.109289	0.256489	0.25276	0.225081	0.187227	0.146732	0.127148	0.11267	0.098307	0.085074	0.085708	0.088629
	8	0.105974	0.244333	0.239204	0.212707	0.176727	0.138446	0.120412	0.106218	0.092308	0.080447	0.080829	0.083832
	9	0.102729	0.231801	0.226482	0.20079	0.166558	0.130606	0.113148	0.10042	0.087273	0.075966	0.075887	0.079432
	10	0.099581	0.220681	0.214664	0.190046	0.157444	0.123443	0.10665	0.094835	0.08252	0.071431	0.072057	0.075128

Table 10: Total efficiency of short distance runs over various energies and distances. For more see Section 4.1.1 and 4.1.4